

# ADVANCED FUNCTIONAL MATERIALS

## Supporting Information

for *Adv. Funct. Mater.*, DOI: 10.1002/adfm.202201256

Metal-Free Organic Triplet Emitters with On–Off  
Switchable Excited State Intramolecular Proton Transfer

*Wenhao Shao, Jie Hao, Hanjie Jiang, Paul M.  
Zimmerman, and Jinsang Kim\**

Supporting Information

**Metal-Free Organic Triplet-Emitters with On-Off Switchable Excited State Intramolecular Proton Transfer**

*Wenhao Shao, Jie Hao, Hanjie Jiang, Paul M. Zimmerman, and Jinsang Kim\**

Prof. J. Kim

Macromolecular Science and Engineering, Department of Materials Science and Engineering,  
and Department of Chemical Engineering

University of Michigan

Ann Arbor, MI 48109, USA

E-mail: jinsang@umich.edu

W. Shao, J. Hao, H. Jiang, Prof. P.M. Zimmerman, Prof. J. Kim

Department of Chemistry

University of Michigan

Ann Arbor, MI 48109, USA

J. Hao

Center of Single-Molecule Sciences

Institute of Modern Optics

College of Electronic Information and Optical Engineering

Nankai University, Tianjin 300071, China

**Contents**

I. Additional experimental details.....	3
1.1 General.....	3
1.2 Physical measurements.....	3
1.3 Solvent vapor annealing.....	3
1.4 Photopatterning and photochromism.....	4
1.5 Statistical Analysis and Data Processing.....	4
1.6 Synthesis of prototype molecules.....	4
II. Computational details.....	7
III. Additional computational results.....	8
Figure S1. Expanded RAS-SF NTO results for HBI (1) and BrA-HBI (2).....	8
Figure S2. Expanded RAS-SF calculation results for HBI (1) and BrA-HBI (2).....	9
Figure S3. RAS-SF calculation results for keto-form molecules.....	10
Figure S4. RAS-SF calculation results for enol-form molecules.....	11
IV. Additional photophysical analyses.....	12
Figure S5. Emission spectra v.s. temperature curve for BrA-HBI (2).....	12
Figure S6. Delayed emission lifetime v.s. temperature curve of BrA-HBI (2).....	13
Figure S7. Photophysical analysis of methylated BrA-HBI (2).....	14
Figure S8. Br-HBI (3) in PS.....	14
Figure S9. Emissive patterns of Br-HBI (3) in P4VP.....	15
Figure S10. Emissive patterns of Br-HBI (3) in PS.....	16
Figure S11. Photophysical analysis of emissive patterns.....	17
V. Extracting delayed emission quantum yield from total quantum yield.....	18
VI. Reported ESIPT molecules with room temperature triplet emission.....	20
VI. RAS-SF frontier molecular orbitals of the prototype molecules.....	22
VII. NMR spectra.....	24
VIII. Mass Spectra.....	31
IX. Reference.....	35

## I. Additional experimental details

### 1.1 General

All chemicals used were purchased from Millipore Sigma or Fisher Scientific and used without further purification unless specified. 4-bromo-2-hydroxybenzaldehyde was purchased from TCI America and ChemScene. Deuterated solvents for NMR spectroscopy (nuclear magnetic resonance) were purchased from Cambridge Isotope Laboratories or Millipore Sigma. Poly(methyl methacrylate) (PMMA) was purchased from Aldrich Chemical Co. ( $M_w \sim 350,000$ ). Poly(acrylic acid) (PAA) was purchased from Aldrich Chemical Co. (lot # MKBR9922V,  $M_w \sim 450,000$ ). Poly(4-vinylpyridine), linear (P4VP) was purchased from Scientific Polymer Products Inc. (lot # 401116018,  $M_w \sim 50,000$ ). Polystyrene (PS) was purchased from Aldrich Chemical Co. (lot # 15902CI,  $M_w \sim 280,000$ ).

### 1.2 Physical measurements

- Nuclear Magnetic Resonance (NMR) spectra were collected on Varian Vnmrs 500 (500 MHz) spectrometer.
- Mass Spectrometry and High Resolution Mass Spectrometry (HRMS) were conducted on Agilent Q-TOF HPLC-MS. Compounds were dissolved in Milli-Q water/acetonitrile (LC/MS grade) (9:1) with a concentration of  $10 \mu\text{M}$  and  $10 \mu\text{L}$  of the solution was injected into the spectrometer. Blank mixed solvent was used as the background. Mass spectra reported in section VIII were obtained by subtracting the background spectra from the sample spectra.
- Photoluminescence spectra were collected on a Photon Technologies International (PTI) QuantaMaster spectrofluorometer (QM-400) equipped with an integrating sphere (K-Sphere) and a cryostat.
- The emitters were doped in PMMA or PAA for solid-state measurements: quartz substrates ( $1.5 \times 2.5 \text{ cm}$ ) were prepared and cleaned by sonication consecutively in soap, deionized water, acetone, isopropyl alcohol, and then proceeded to UV-ozone treatment for 30 min. THF/chloroform (1:1 vol.:vol.) solution containing emitter (1 wt% to polymer) and 2.5 wt% PMMA, or ethanol solution containing emitter (1 wt% to polymer) and 2.5 wt% PAA were prepared and spin-coated on the cleaned quartz substrates (500 rpm for 5 min). Last, the films were transferred into a glovebox filled with  $\text{N}_2$  and baked at  $120 \text{ }^\circ\text{C}$  for 30 min. Films were stored in the glovebox except during measurements.
- For absolute quantum yield measurements, blank PMMA or PAA films were used as background.

### 1.3 Solvent vapor annealing

The emitters were doped in P4VP or PS for solvent vapor annealing and photophysical measurements: quartz ( $1.5 \times 2.5 \text{ cm}$ ) or glass ( $1.5 \times 1.5 \text{ cm}$ ) substrates were prepared and cleaned by sonication consecutively in soap, deionized water, acetone, isopropyl alcohol, and then proceeded to UV-ozone treatment for 30 min. Chloroform solution containing Br-HBI (1 wt% to polymer) and 1.25 wt% polymer were prepared and spin-coated on the cleaned substrates (500 rpm for 5 min). The prepared films were dried under vacuum for at least 20 minutes to ensure complete evaporation of solvent. Solvent vapor annealing was carried out in an empty vacuum desiccator: the sample and a 25 mL beaker containing concentrated HCl (10 mL) were placed in a petri-dish at the center of the metal plate. The chamber was closed and vacuumed for an initial 2 minutes for the stabilization of HCl vapor. Then, the stop cock connected with the vacuum was closed and the vacuum in the desiccator was maintained for an additional 8 minutes.

### 1.4 Photopatterning and photochromism

The emitters were doped in P4VP or PS on cleaned glass substrates following the same procedure. The samples were transferred to a N<sub>2</sub>-filled glovebox and were covered with a photomask made of Molybdenum by Towne Technologies, Inc. A 254 nm hand-held UV lamp (purchased from Fisher Scientific) with a low power density of 2.4 mW/cm<sup>2</sup> was used to generate the photopattern. The samples were subsequently baked on a hot plate at various temperatures selected. Note that samples were placed upside-down (polymer film in contact with the hot plate) during the baking process to prevent bubble formation. A Canon EOS 550d camera was used to record the emission of the films illuminated with a 365 nm hand-held UV lamp, before photopatterning, directly after photopatterning, and after baking.

### 1.5 Statistical Analysis and Data Processing

- All data were processed and plots were generated in Origin Pro 2017.
- Steady state emission and excitation spectra were smoothed with the built-in Savitzky-Golay method (Points of Window: 20; Polynomial Order: 3), and were plotted either as lines or shades.
- Lifetime decay profiles (e.g. Figure 2c and 5b) were plotted without any data pre-processing.
- Phosphorescence emission spectra were plotted as dots due to the high signal/noise ratio without any data pre-processing.
- Quantum yields in Figure 4 and elsewhere in the manuscript were averaged among three film samples. The mean and standard error included in Figure 4 were calculated by Origin Pro 2017.

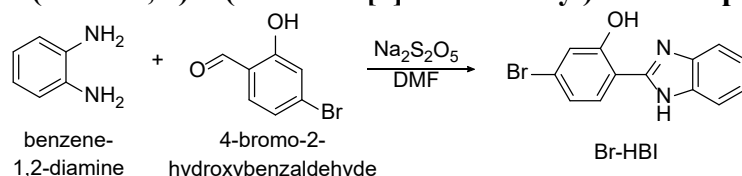
### 1.6 Synthesis of prototype molecules

Purity of the compounds synthesized were confirmed by NMR and MS/HRMS, as documented in section VII and VIII.

#### ■ (HBI, 1) 2-(1*H*-benzo[*d*]imidazol-2-yl)phenol

HBI was purchased from Millipore Sigma and used without further purification.

#### ■ (Br-HBI, 3) 2-(1*H*-benzo[*d*]imidazol-2-yl)-5-bromophenol

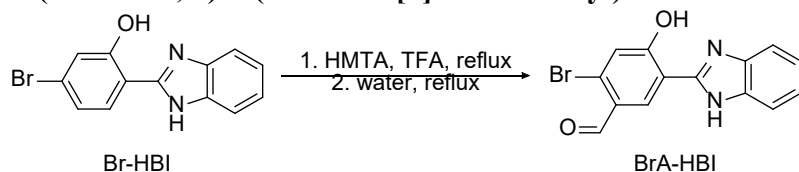


To a single-neck 500 mL round bottom flask with a stirring solution of benzene-1,2-diamine (9.95 mmol, 1 equiv.) and 4-bromo-2-hydroxybenzaldehyde (9.95 mmol, 1 equiv.) in DMF (200 mL, ~0.05 mL/mmol benzaldehyde), sodium metabisulfite (1.99 mmol, 0.2 equiv.) was added. The mixture was stirred for 6–8 h at 110 °C. Color of the mixture turned gradually to green and dark brown at the end. After the reaction was completed, the mixture was poured into cold DI water under stirring. The resulting solid (pink/red) was further purified by column chromatography on silica gel (eluent: hexane/ethyl acetate, 30:1 to 4:1) to afford a pale yellow solid (1.7g, 60%).

- <sup>1</sup>H NMR (500 MHz, DMSO-*d*<sub>6</sub>) δ 13.41 (s), 8.00 (d, *J* = 8.4 Hz, 1H), 7.67 (s, 2H), 7.30 (dt, *J* = 6.1, 3.6 Hz, 2H), 7.27 (d, *J* = 2.0 Hz, 1H), 7.24 (dd, *J* = 8.4, 2.0 Hz, 1H).
- <sup>13</sup>C NMR (126 MHz, DMSO-*d*<sub>6</sub>) δ 159.27, 151.32, 128.27, 124.70, 122.65, 120.34, 112.59.
- HRMS [M+H]<sup>+</sup>
  - Predicted *m/z*: 289.00 (100.0%), 291.00 (98.5%), 290.00 (14.2%), 292.00 (13.8%), 293.00 (1.2%)

- Found m/z: 288.9968 (100%), 290.9949 (97.7%), 288.9998 (14.5%), 291.9977 (14.4%)

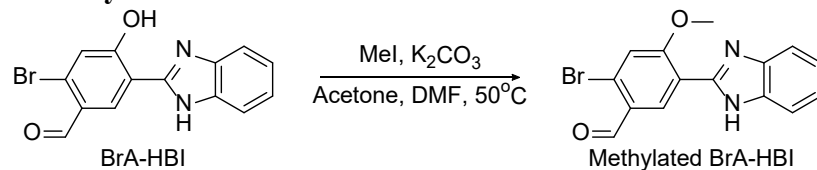
■ **(BrA-HBI, 2) 5-(1H-benzo[d]imidazol-2-yl)-2-bromo-4-hydroxybenzaldehyde**



In a 100 mL double-neck round bottom flask, the previously synthesized Br-HBI (3.35 mmol, 1 equiv.) and hexamethylenetetramine (HMTA, 33.5 mmol, 10 equiv.) were added followed by the addition of trifluoroacetic acid (TFA, 35 mL). After degassing the mixture with Ar, it was heated at reflux for 5 h, during which the initial white slurry turned into clear yellow solution. Prolonged reaction time had no obvious side effects and might help increase the yield of para aldehyde-substituted products v.s. ortho products. 2. Afterwards, DI water (~ 30 mL) was added and the mixture was refluxed for another 1 h. Then the reaction was stopped and left in the refrigerator overnight. The solid precipitate formed was filtered and washed with water. The obtained crude product was purified by column chromatography on silica gel (dry-loading, eluent: hexane/ethylacetate, 20:1 to 1:1; product was obtained near 9:1-6:1) to afford a pale yellow solid (93 mg).

- $^1\text{H NMR}$  (500 MHz, DMSO- $d_6$ )  $\delta$  10.12 (s, 1H), 8.67 (s, 1H), 7.70 (dd,  $J = 6.0, 3.2$  Hz, 2H), 7.41 (s, 1H), 7.34 (dd,  $J = 6.0, 3.1$  Hz, 2H).
- $^{13}\text{C NMR}$  (126 MHz, DMSO- $d_6$ )  $\delta$  190.16, 164.56, 150.34, 129.44, 129.02, 125.08, 123.97, 122.64, 115.38, 113.20.
- HRMS  $[\text{M}+\text{H}]^+$ 
  - Predicted m/z: 316.99 (100.0%), 318.99 (97.4%), 319.99 (15.5%), 318.00 (15.3%), 319.00 (1.5%), 321.00 (1.1%)
  - Found m/z: 316.9916 (100%), 318.9898 (97.6%), 317.9940 (15.3%), 319.9926 (15.7%)

■ **Methylation of BrA-HBI**

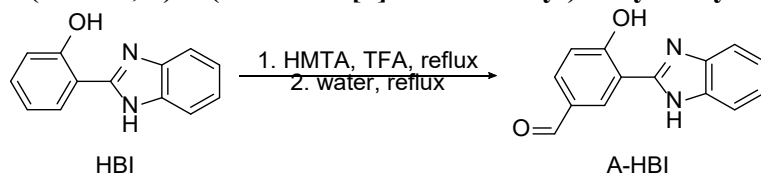


In a 10 mL round bottom flask, the mixture of BrA-HBI (4.337 mg, 13.68  $\mu\text{mol}$ ), powdered  $\text{K}_2\text{CO}_3$  (5.900 mg, 3.121 equiv.), and methyl iodide (MeI, a few drops, in excess) in acetone (3 mL) + DMF (1 mL) mixed solvent (DMF could be used solely) was stirred at 60°C under Ar atmosphere for several days. The reaction was slow due to the low reactivity of BrA-HBI.  $\text{K}_2\text{CO}_3$  (5.9 mg) and MeI (a few drops) were added in the middle of the reaction to fully convert the unreacted BrA-HBI to the product. When the starting material disappeared on TLC, the solution was poured into water to obtain the crude product, which was further purified by multiple reprecipitations in water/methanol mixture to obtain the pure product as a white powder (0.99 mg).

- $^1\text{H NMR}$  (400 MHz, DMSO- $d_6$ )  $\delta$  12.29 (s, 1H), 10.18 (s, 1H), 8.81 (s, 1H), 7.71 – 7.67 (m, 1H), 7.66 (s, 1H), 7.62 (dd,  $J = 6.7, 1.7$  Hz, 1H), 7.27 – 7.19 (m, 2H), 4.17 (s, 3H).
- HRMS  $[\text{M}+\text{H}]^+$

- Predicted m/z: 331.01 (100.0%), 333.01 (99.0%), 332.01 (17.2%), 334.01 (16.0%), 335.01 (1.7%)
- Found m/z: 331.0075 (100%), 333.0056 (98.9%), 332.0102 (16.9%), 334.0084 (16.5%)

▪ (A-HBI, 4) 3-(1*H*-benzo[*d*]imidazol-2-yl)-4-hydroxybenzaldehyde



A-HBI was synthesized from HBI using the same procedure as BrA-HBI. Yield: 100 mg, 12.6%.

- $^1\text{H}$  NMR (500 MHz, DMSO-*d*<sub>6</sub>)  $\delta$  13.88 (s), 9.93 (s, 1H), 8.69 (d, *J* = 1.6 Hz, 1H), 7.95 (dd, *J* = 8.5, 1.6 Hz, 1H), 7.70 (dd, *J* = 5.4, 3.3 Hz, 2H), 7.32 (dd, *J* = 6.0, 3.1 Hz, 2H), 7.23 (d, *J* = 8.5 Hz, 1H).
- $^{13}\text{C}$  NMR (126 MHz, DMSO-*d*<sub>6</sub>)  $\delta$  191.30, 163.68, 151.05, 133.98, 128.80, 128.77, 123.69, 118.45, 113.67.
- HRMS [*M*+*H*]<sup>+</sup>
  - Predicted m/z: 239.08 (100.0%), 240.09 (15.3%), 241.09 (1.5%)
  - Found m/z: 239.0815 (100%), 240.0841 (15.8%)

## II. Computational details

The RAS-SF method is programmed in the Q-Chem 5.4 software package<sup>[1]</sup>, and the SOC computations are implemented in a development version of Q-Chem. All RAS-SF calculations were performed with the 6-31G\* basis set<sup>[2]</sup> and the RIMP2-cc-pVDZ auxiliary basis<sup>[3]</sup>. RAS-SF hole, particle calculations with 8 electron in 8 orbital active spaces were carried out with RAS1 and RAS3 subspaces including all occupied and virtual orbitals, respectively. Unless otherwise stated, the core electrons were kept frozen. Reference orbitals for RAS-SF were obtained from restricted open-shell density functional theory (RODFT) using the B3LYP functional in the nonet state. Geometries of the molecules were optimized at the ground state using  $\omega$ B97X-D functional<sup>[4]</sup> and the def2-TZVP basis set<sup>[5]</sup>. Calculations of SOC constants utilize general libraries developed for SOC calculations within EOM-CC<sup>[6]</sup>. Spin-orbit NTOs were computed and analyzed using the libwfa library<sup>[7]</sup>. The NTOs with the largest singular values, for each compound, were plotted using Molden program<sup>[8]</sup>.



## III. Additional computational results

	 HBI ( <b>1</b> -enol)	 HBI ( <b>1</b> -keto)	 BrA-HBI ( <b>2</b> -enol)	 BrA-HBI ( <b>2</b> -keto)
$S_0 \leftrightarrow T_1$ SOCME	 $(\pi, \pi^*)$ 0.57	 $(\pi, \pi^*)$ 11.74	 $(n, \pi^*)$ 53.33	 $(n, \pi^*)$ 71.43
$S_1 \leftrightarrow T_1$ SOCME	 $(\pi, \pi^*)$ 1.50	 $(\pi, \pi^*)$ 0.62	 $(n, n)$ 0.44	 $(\pi, \pi^*)$ 0.43
$S_1 \leftrightarrow T_2$ SOCME	 $(\pi, \pi^*)$ 0.14	 $(\pi, \pi^*)$ $(n, \pi^*)$ 10.46	 $(n, \pi^*)$ 58.99	 $(n, \pi^*)$ 31.23

**Figure S1. Expanded RAS-SF NTO results for HBI (1) and BrA-HBI (2)** Relevant orbitals of HBI and BrA-HBI in their enol or keto forms; RAS-SF natural transition orbitals of significant S-T transitions are displayed, along with their SOC constants (units in  $\text{cm}^{-1}$ ) and the corresponding transition characters.

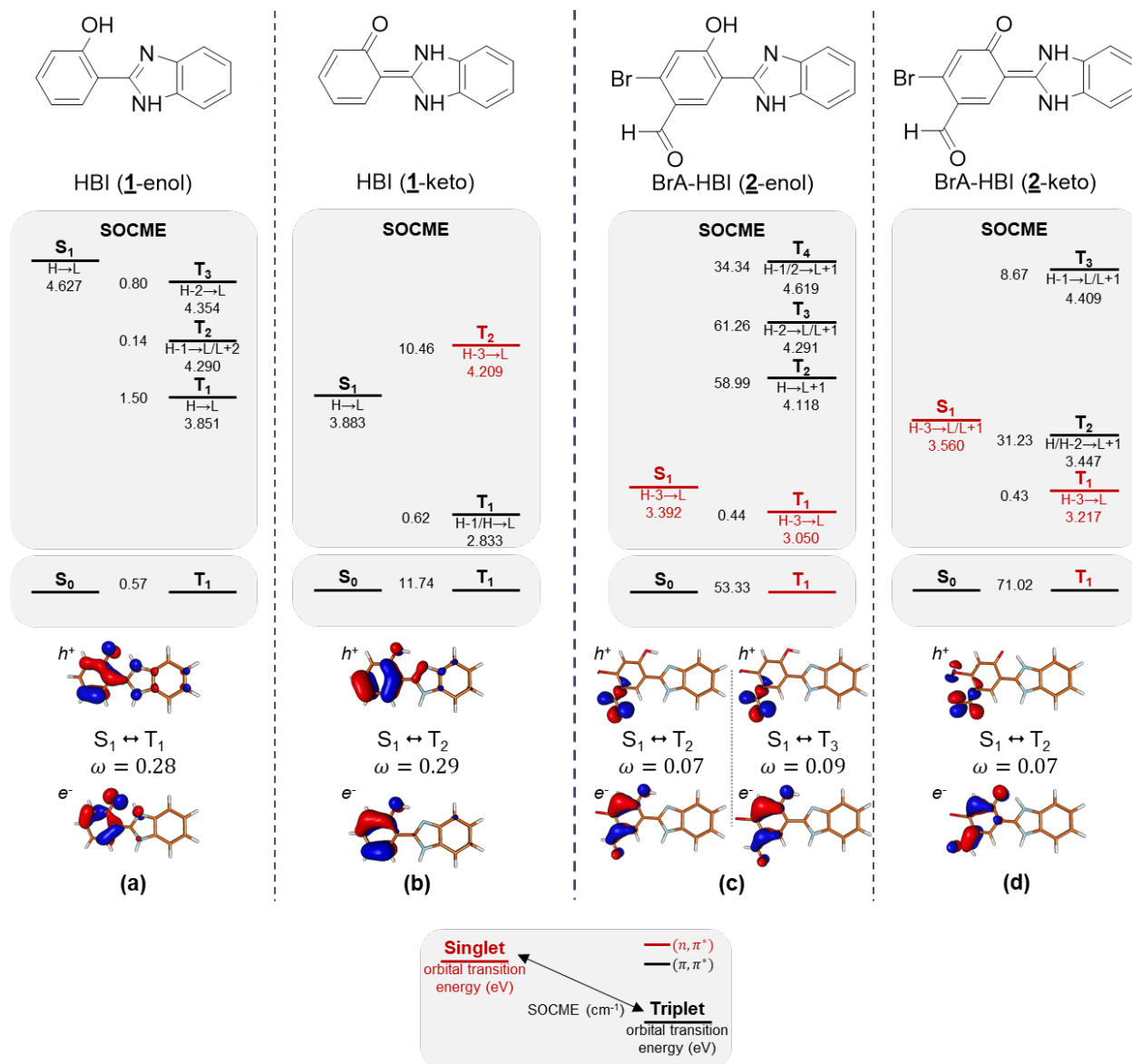


**Figure S2. Expanded RAS-SF calculation results for HBI (1) and BrA-HBI (2) showing the orbital configurations:** Chemical structures of HBI and BrA-HBI in their enol or keto forms; RAS-SF calculation results for the selected excited states, their energies (units in eV), transition character, and SOCMEs (units in  $\text{cm}^{-1}$ ) between  $S_1$  and triplet states (see the legend for details). RAS-SF natural transition orbitals of the S-T transitions with largest SOCME are displayed.  $\omega$  represents the singular values of the transitions shown in the NTO pairs, indicating the significance of the specified orbital transitions. Selected frontier molecular orbitals were attached in section VI.

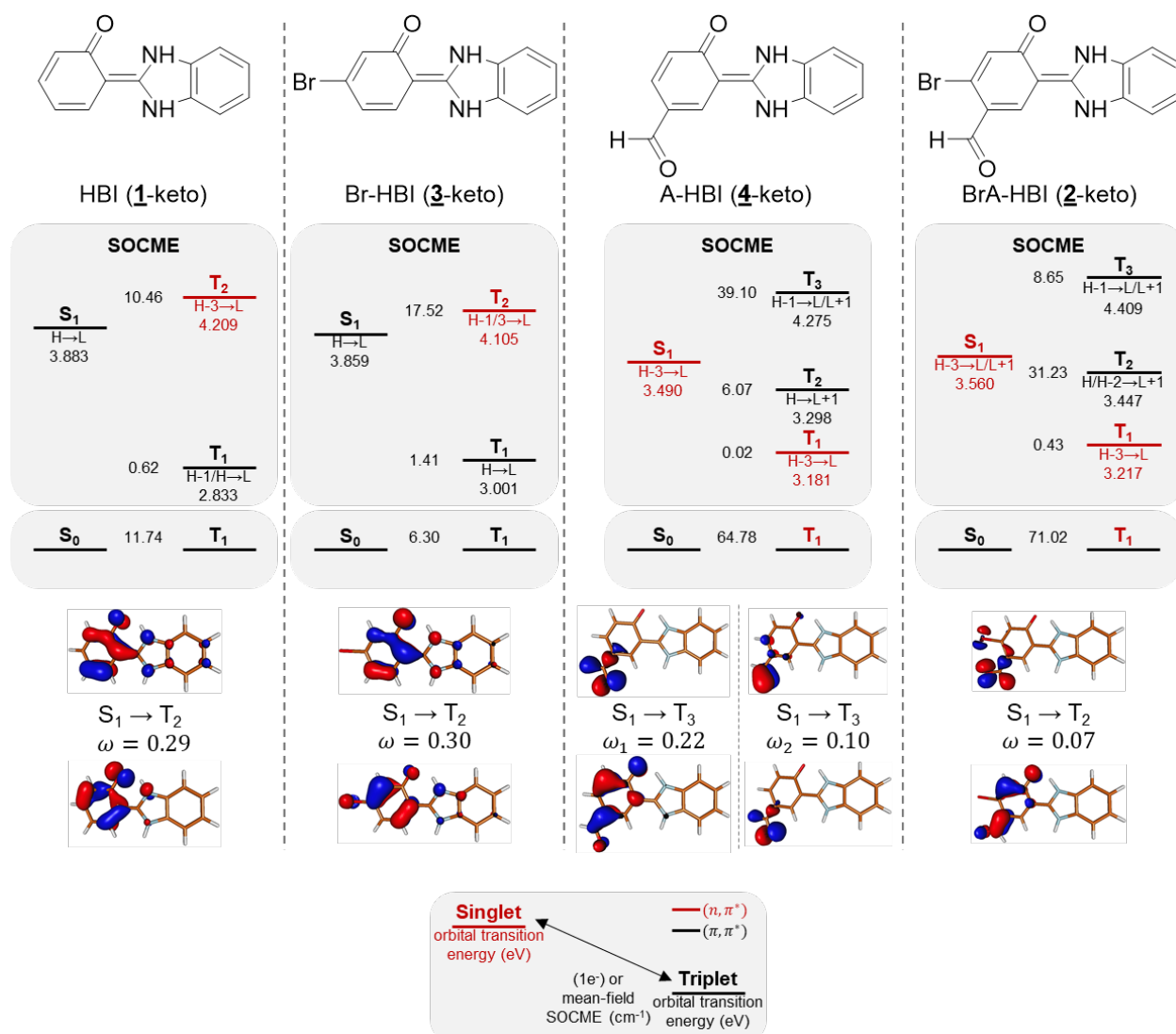


**Figure S3. RAS-SF calculation results for keto-form molecules** Chemically structures of HBI, Br-HBI, A-HBI, and BrA-HBI in their keto form; RAS-SF calculation results for the selected excited states, their energies, transition character, SOCMEs between  $S_1$  and triplet states, and SOCMEs between  $T_1$  and  $S_0$  (see the legend for details). RAS-SF natural transition orbitals of the S-T transitions with largest SOCME are displayed.  $\omega$  represents the singular values of the transitions shown in the NTO pairs, indicating the significance of the specified orbital transitions. In some cases (A-HBI), two NTO pairs are shown, both having large  $\omega$  values. Selected frontier molecular orbitals were attached in section VI.

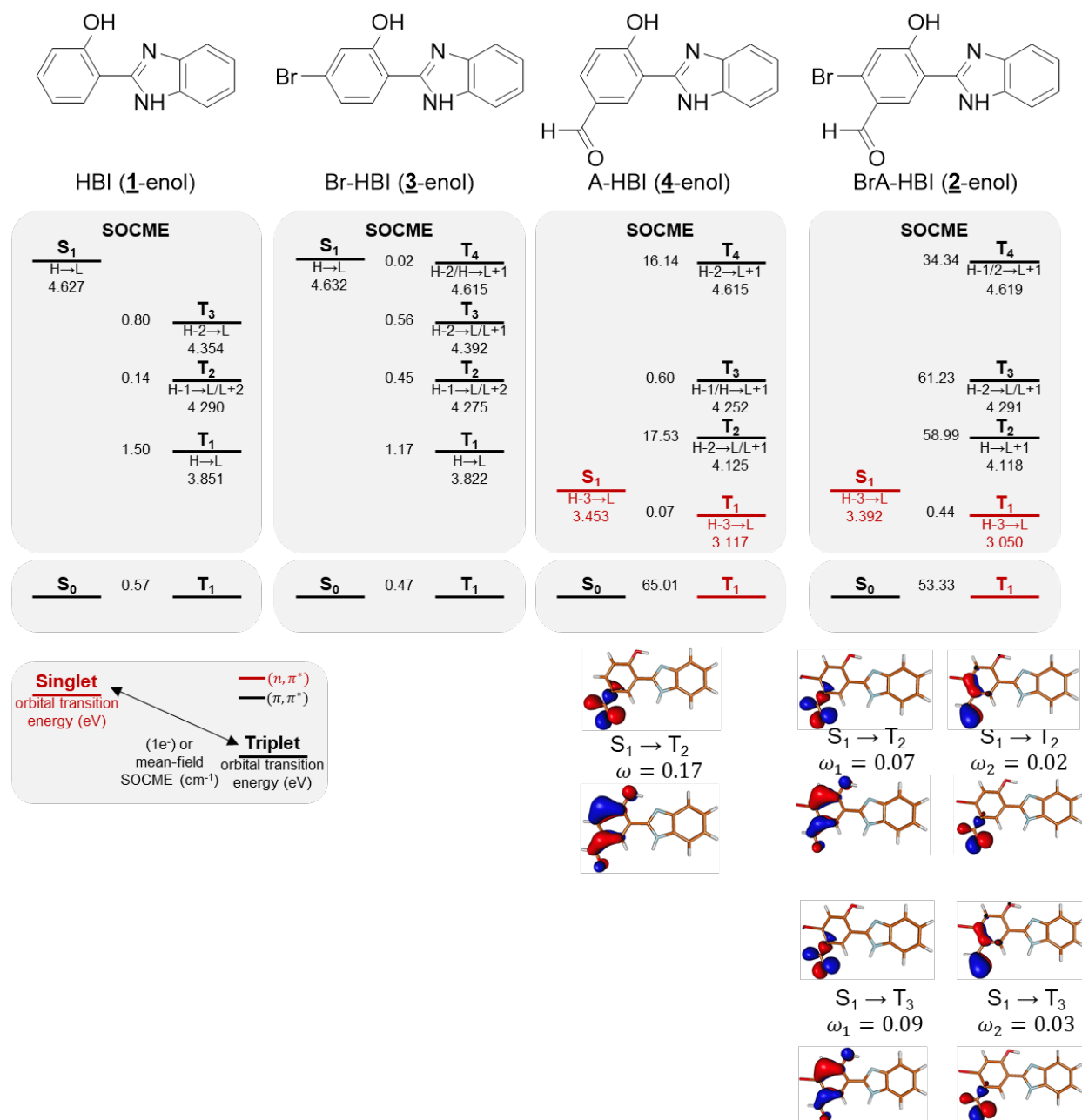


**Figure S4. RAS-SF calculation results for enol-form molecules** Chemically structures of HBI, Br-HBI, A-HBI, and BrA-HBI in their enol form; RAS-SF calculation results for the selected excited states, their energies, transition character, SOCMEs between S<sub>1</sub> and triplet states, and SOCMEs between T<sub>1</sub> and S<sub>0</sub> (see the legend for details). RAS-SF natural transition orbitals of the S-T transitions with largest SOCME are displayed. ω represents the singular values of the transitions shown in the NTO pairs, indicating the significance of the specified orbital transitions. In some cases (BrA-HBI), two NTO pairs under the same transition are shown, both having large ω values. Selected frontier molecular orbitals were attached in section VI.

## IV. Additional photophysical analyses

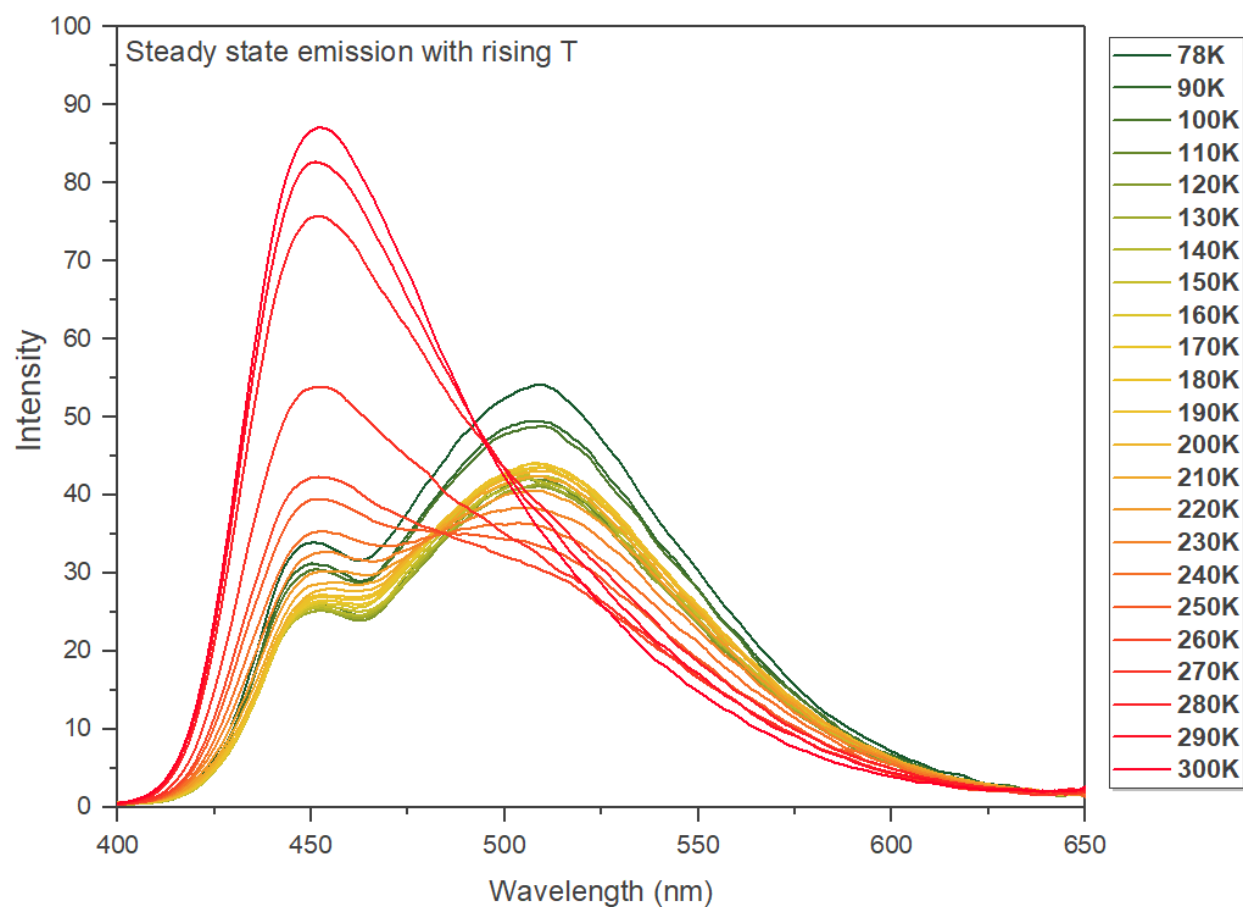


**Figure S5. Emission spectra v.s. temperature curve for BrA-HBI (2)** Steady state emission spectra of BrA-HBI in spin-coated PMMA film with 1 wt% doping concentration, measured in vacuum with rising temperature.

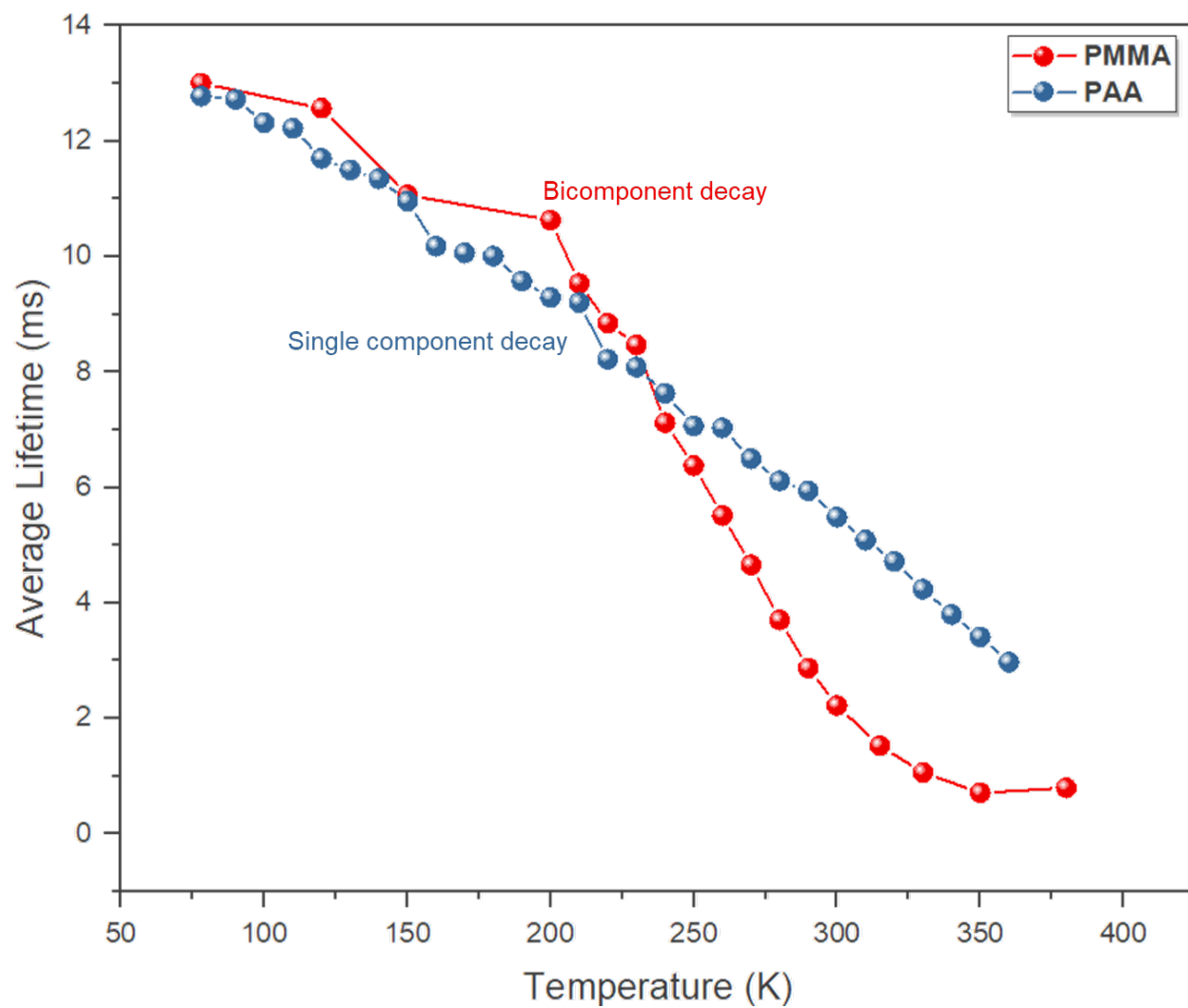


**Figure S6.** Delayed emission lifetime v.s. temperature curve of BrA-HBI (2) in spin-coated PMMA or PAA film with 1 wt% doping concentration, measured in vacuum with rising temperature.

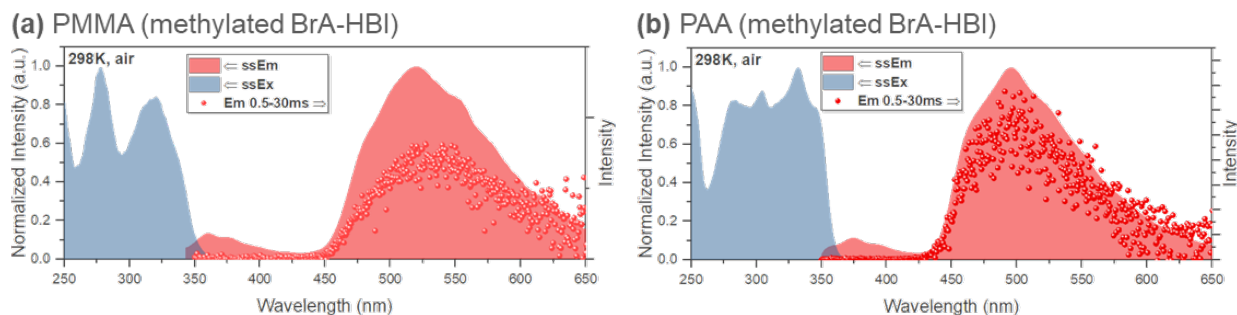


**Figure S7. Photophysical analysis of methylated BrA-HBI (2)** Steady state excitation (filled), emission spectra (filled), and delayed emission spectra (dots) of methylated BrA-HBI in spin-coated (a) PMMA or (b) PAA films with 1 wt% doping concentration measured at 298K.

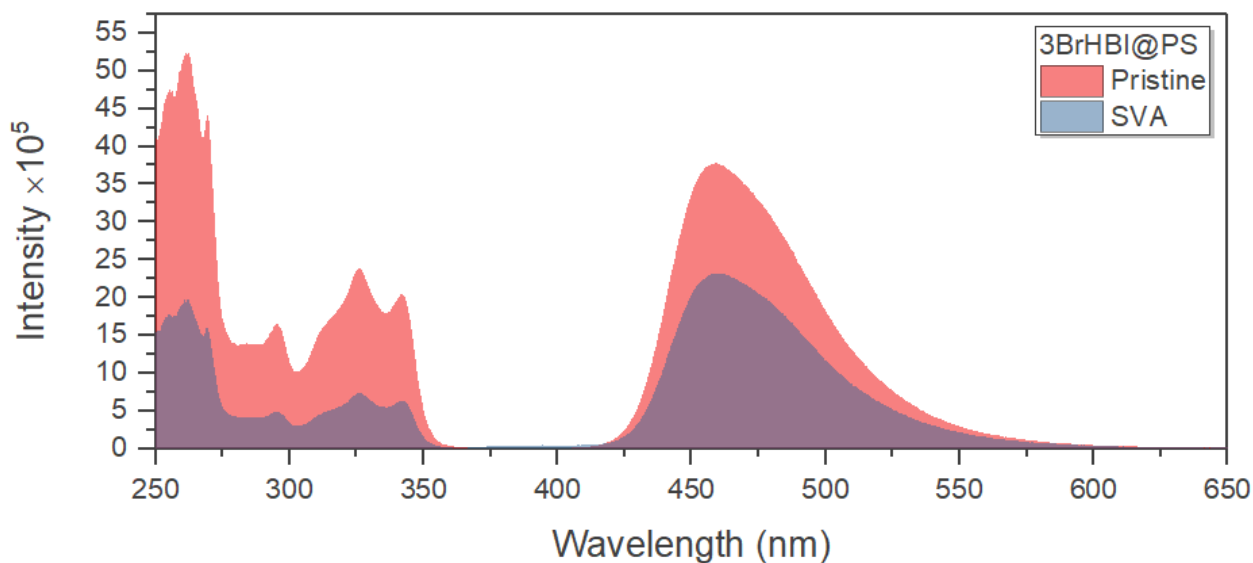


**Figure S8. Br-HBI (3) in PS.** Steady state emission spectra of Br-HBI in PS (spin-coated, 1 wt% doping) upon solvent vapor annealing (SVA) with concentrated HCl.

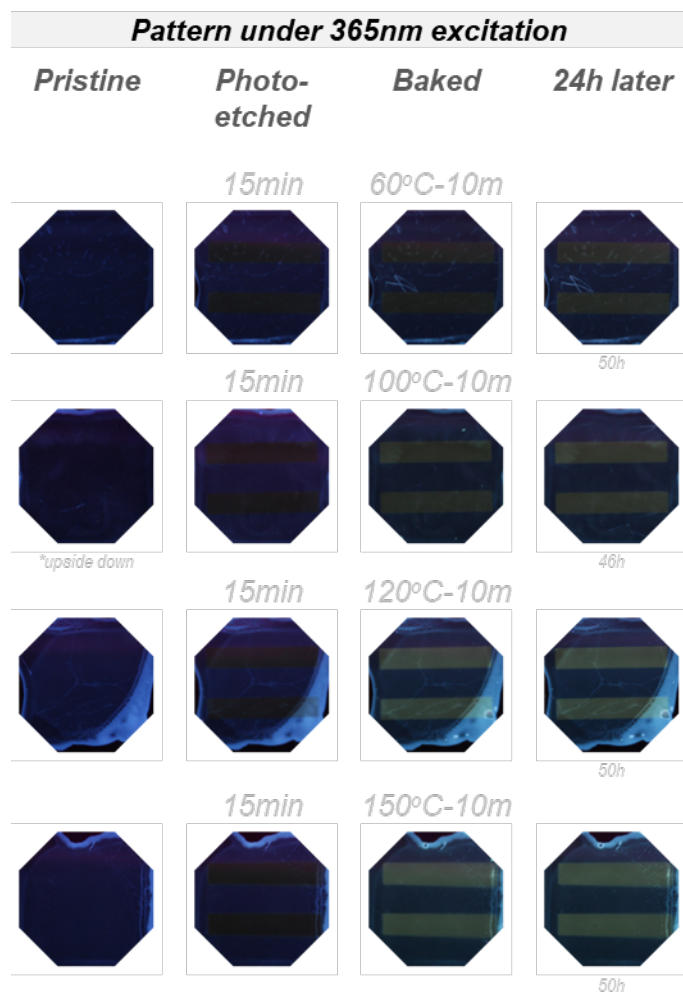


**Figure S9. Emissive patterns of Br-HBI (3) in P4VP** under 365 nm illumination created by i) photo-etching with 254 nm UV lamp and a mask for 15 minutes, followed by ii) baking at various temperatures for 10 minutes.



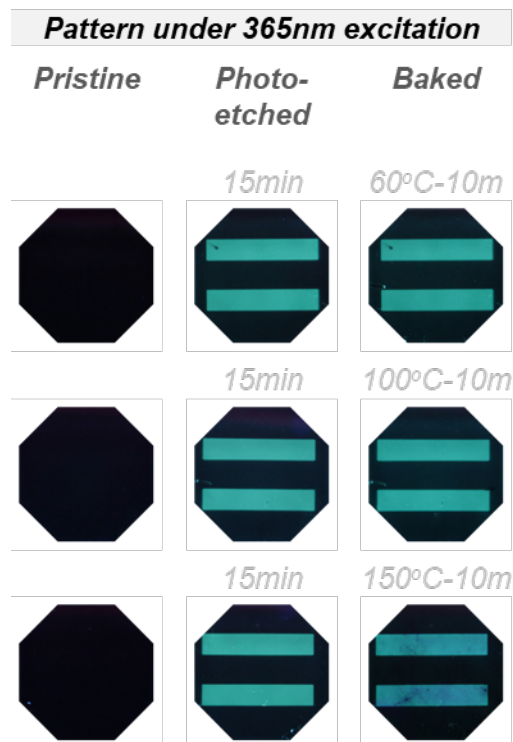


**Figure S10. Emissive patterns of Br-HBI (3) in PS** under 365 nm illumination created by i) photo-etching with 254 nm UV lamp and a mask for 15 minutes, followed by ii) baking at various temperatures for 10 minutes.

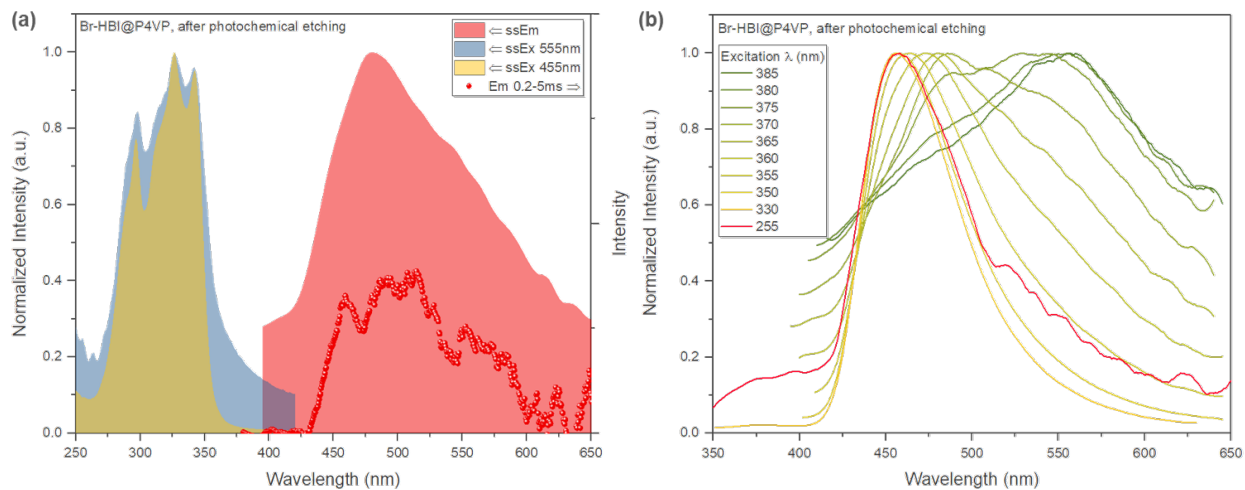


**Figure S11. Photophysical analysis of emissive patterns.** (a) Steady state excitation (filled), emission spectra (filled), and delayed emission spectra (dots) of Br-HBI in P4VP (spin-coated, 1 wt% doping) after photo-etching with 254 nm UV lamp for 15 minutes; panel (b) displays the steady state emission spectra with various excitation wavelengths.

## V. Extracting delayed emission quantum yield from total quantum yield

In this section, we will explain how to deconvolute the total quantum yield ( $\Phi_{tot}$ ) into prompt fluorescence ( $\Phi_{PF}$ ) and delayed emission quantum yield ( $\Phi_{delay}$ ) as shown in Fig. 4.

For HBI, A-HBI, Br-HBI, and BrA-HBI in PAA matrix, deconvolution could be simply done from the steady state emission spectra since prompt fluorescence and delayed emission, in the form of phosphorescence, could be easily distinguished.

In the PMMA matrix at room temperature, the steady state emission spectra were complicated by prompt and delayed emission, which overlapped with each other. However, we could use the steady state emission intensity in air v.s. in vacuum, assisted by the delayed emission intensity in air v.s. in vacuum, to deconvolute  $\Phi_{delay}$  from  $\Phi_{tot}$ . The procedure is documented as follows:

### 1) Data acquisition

First, the steady state and delayed emission spectra in air and in vacuum are obtained as well as the delayed emission decay curve in air and in vacuum. Steady state emission spectra of a blank PMMA film fabrication under the same procedure was measured as the background. Delayed emission spectra didn't need additional background information since PMMA was optically inert in our excitation range and scattered incident light has been gated. and Spin-coated PMMA thin films were quite susceptible to oxygen permeation, and thus deprivation of oxygen under vacuum would restore the total emission profile, both in the steady state and delayed regime.

### 2) Integration of emission intensity

After subtracting the background spectra from blank PMMA films, the steady state emission spectra in air and in vacuum were integrated to obtain  $I_{ss,air}$  and  $I_{ss,vac}$ . Using the same integration range, delayed emission spectra were integrated without background subtraction to obtain  $I'_{d,air}$  and  $I'_{d,vac}$ . Since a gated time range was applied during delayed emission measurement (e.g. 0.2-10 ms),  $I'_{d,air}$  and  $I'_{d,vac}$  were not the total delayed emission intensity and therefore not comparable and needed to be corrected using the fitted decay curve.

### 3) Decay fitting and extrapolation

The decay curves in air and in vacuum were fitted using the embedded multi-exponent fitting module of QuantaMaster (data acquisition and analysis software from PTI). Using the fitting parameters, the original decay curves were extrapolated to 1  $\mu$ s and 1 s, assuming that this range would cover most of the delayed contents and make  $I_{d,air}$  and  $I_{d,vac}$  comparable. The tail of the decay curves (1 s) could be easily fitted with various softwares (QuantaMaster, OriginalPro, etc.); however, extra discretion was needed to fit the head (1  $\mu$ s) of the decay curve in air, which usually exhibit multi-exponent profile in contrast to the decay curve in vacuum. Misleading short decay species ( $\tau < 20 \mu$ s) could exist in the final fitting results even though the measured time range (usually 0.2-10 ms) couldn't cover these short decay species.

As a result, the fitted decay curves could be integrated with the time range chosen for delayed emission spectra measurement (e.g. 0.2-10 ms) and the "full intensity range" (1  $\mu$ s - 1 s). The ratio,  $I_{1\mu s-1s}/I_{0.2-10ms}$  was used to correct the delayed emission intensity,  $I'_{d,air}$  and  $I'_{d,vac}$ . In other words,

$$I_{d,air} = I'_{d,air} \frac{I_{1\mu s-1s}}{I_{0.2-10ms}}, I_{d,vac} = I'_{d,vac} \frac{I_{1\mu s-1s}}{I_{0.2-10ms}}$$

Where  $I_{d,air}$  and  $I_{d,vac}$  are the corrected delayed emission intensity.

#### 4) Extracing $\Phi_{delay}$ and $\Phi_{PF}$

We assume that prompt fluorescence intensity,  $I_{PF}$ , didn't change from air to vacuum. Thus,

$$I_{ss,vac} = I_{d,vac}^* + I_{PF}$$

$$I_{ss,air} = I_{d,air}^* + I_{PF}$$

Note that we used  $I_{d,air}^*$  and  $I_{d,vac}^*$  here to be distinguished from  $I_{d,air}$  and  $I_{d,vac}$  since steady state and delayed emission were measured using different detectors. Thus, we could derive

$$\frac{I_{ss,vac} - I_{ss,air}}{I_{d,vac}^*} = \frac{I_{d,vac}^* - I_{d,air}^*}{I_{d,vac}^*} = \frac{I_{d,vac} - I_{d,air}}{I_{d,vac}}$$

Therefore,

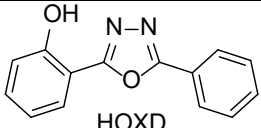
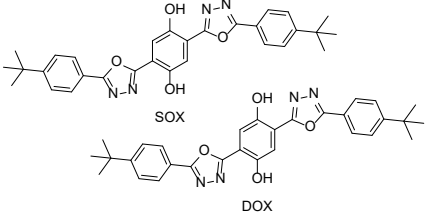
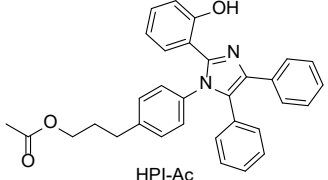
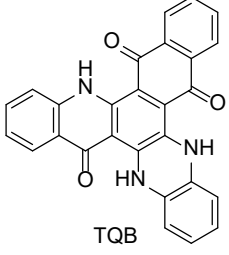
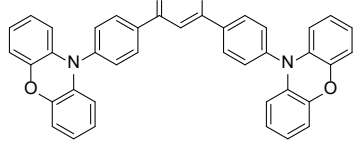
$$\Phi_{delay,vac} = \Phi_{tot,vac} \frac{I_{d,vac}^*}{I_{ss,vac}}$$

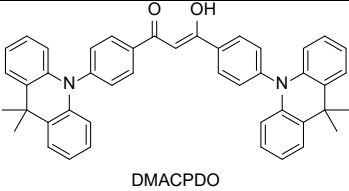
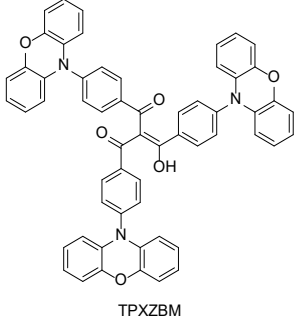
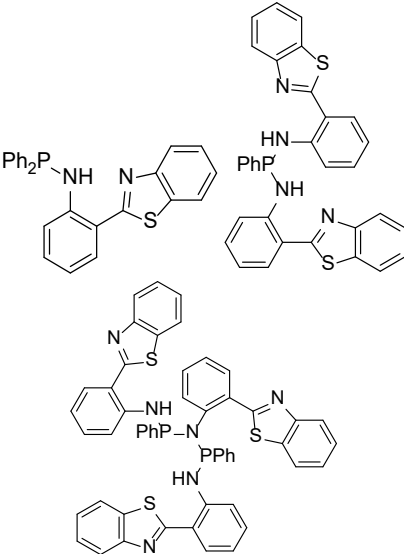
$$\Phi_{PF} = \Phi_{tot} - \Phi_{delay}$$

## VI. Reported ESIPT molecules with room temperature triplet emission

Table S1 listed the contemporary ESIPT emitters that exhibited triplet emission potential. As shown here, room-temperature triplet emission, either in the form of room-temperature phosphorescence (RTP) or thermal assisted delayed fluorescence (TADF) were very rarely observed prior to 2017, nor were their photophysical properties systematically studied. The first tailor-designed ESIPT TADF emitter was made by Adachi group in 2017,<sup>[9]</sup> but the photoluminescence quantum yield of the delayed emission did not exceed 10% due to insufficient reverse intersystem crossing. Since then, study of ESIPT TADF emitters mushroomed and the delayed emission quantum yield was pushed to 42%.<sup>[10]</sup> However, all of these pioneer studies are based on the keto form of ESIPT molecules, and no reports on activating triplet emission from enol form is reported to the best of our knowledge. In addition, activating efficient RTP from ESIPT emitters is rarely explored.

**Table S1. Reported ESIPT molecules with room temperature triplet emission**

	Compound	Type of emission	$\Phi_{delayed}$	Year ref.
1	 HOXD	RTP	Unreported	2002 [11]
2	 SOX DOX	RTP	Unreported	2007 [12]
3	 HPI-Ac	TADF	Unreported	2007 [13]
4	 TQB	TADF	9.5% <sup>a</sup>	2017 [9]
5	 PXZPDO	TADF	36% <sup>b</sup>	2018 [10]

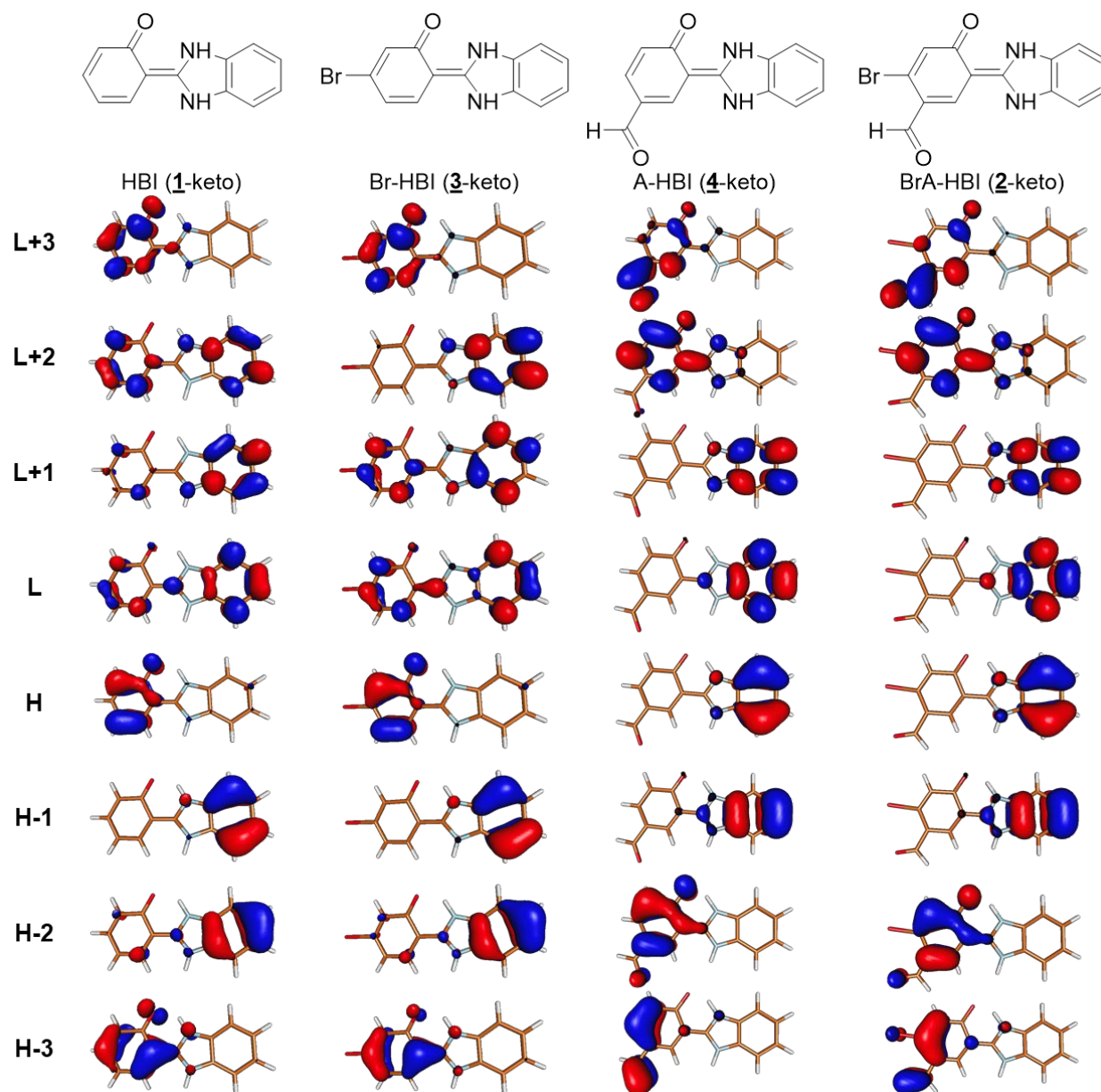
6	 <p>DMACPDO</p>	TADF	42% <sup>b</sup>	2018 [10]
7	 <p>TPXZBM</p>	TADF	4.5% <sup>b</sup>	2021 [14]
8		RTP	<1% <sup>c</sup>	2021 [15]

<sup>a</sup>Measured at 300K, doped in bis[2-(diphenyl- phosphino)phenyl]ether oxide (DPEPO) host.

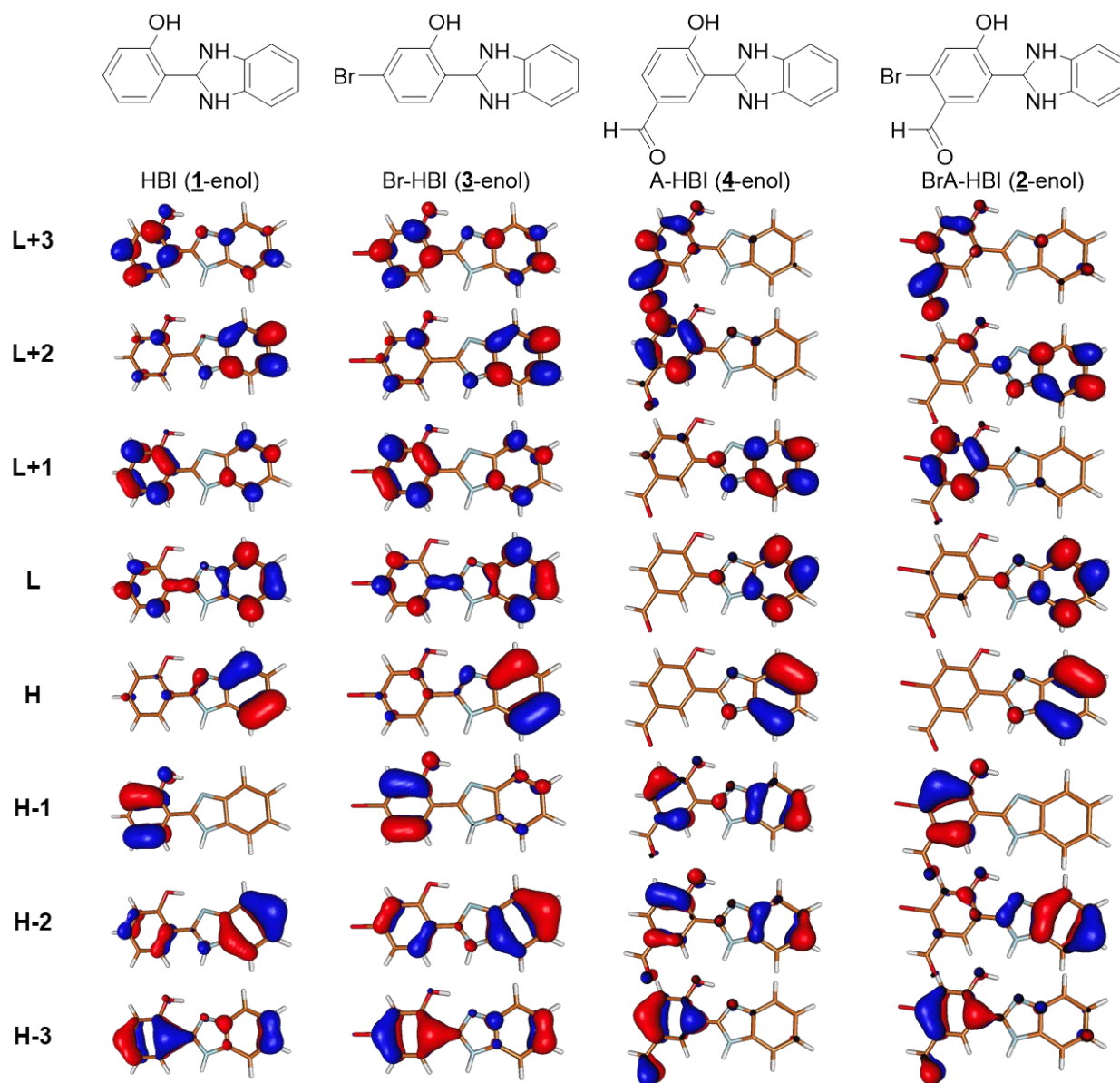
<sup>b</sup>Measured at 300K, doped in 4,4'-di(9H-carbazol-9-yl)-1,1'-biphenyl (CBP) host.  $\Phi_{delayed}$  was calculated using the total PLQY ( $\Phi_{PL}$ ) and delayed fluorescence weight factor ( $R_d$ ) provided in the original reports.

<sup>c</sup>Measured at 300K in undoped crystals.

## VI. RAS-SF frontier molecular orbitals of the prototype molecules



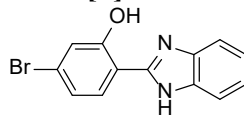
**Figure S12.** Selected frontier molecular orbitals in the keto form calculated by RAS-SF methods. H: HOMO, L: LUMO.



**Figure S13.** Selected frontier molecular orbitals in the enol form calculated by RAS-SF methods. H: HOMO, L: LUMO.



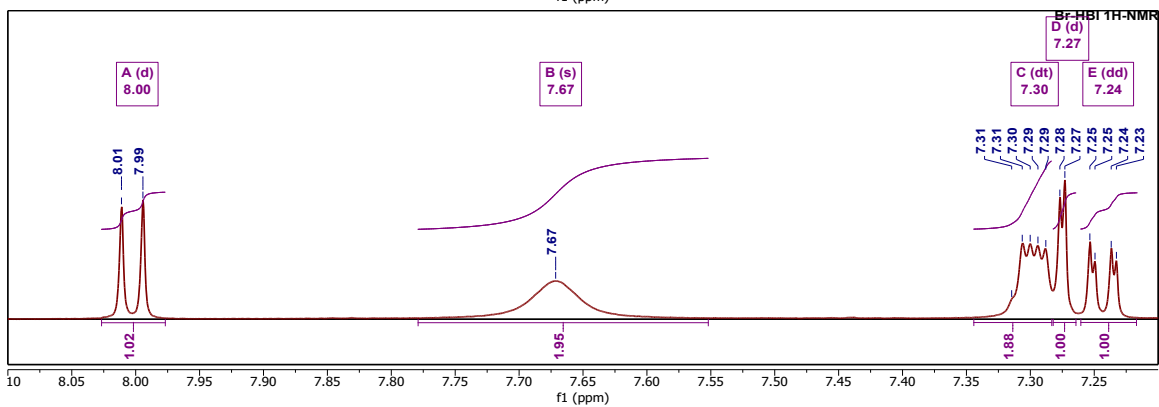
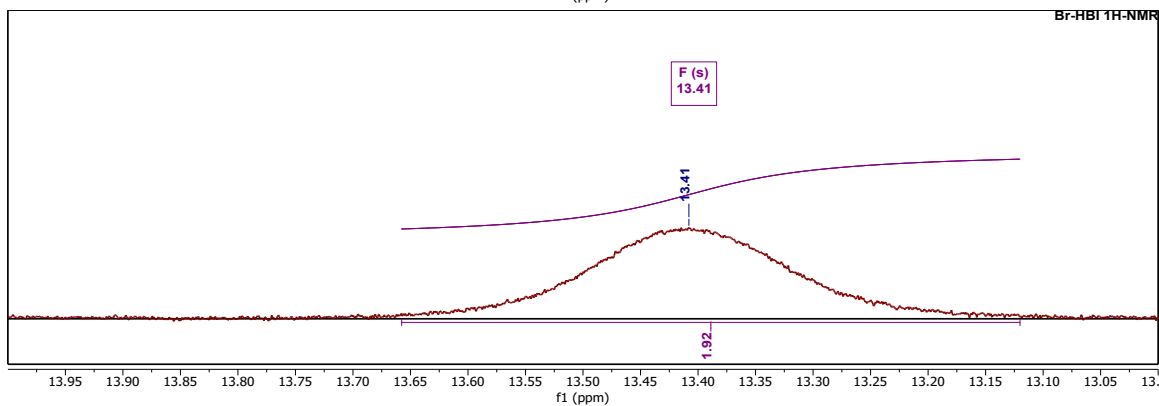
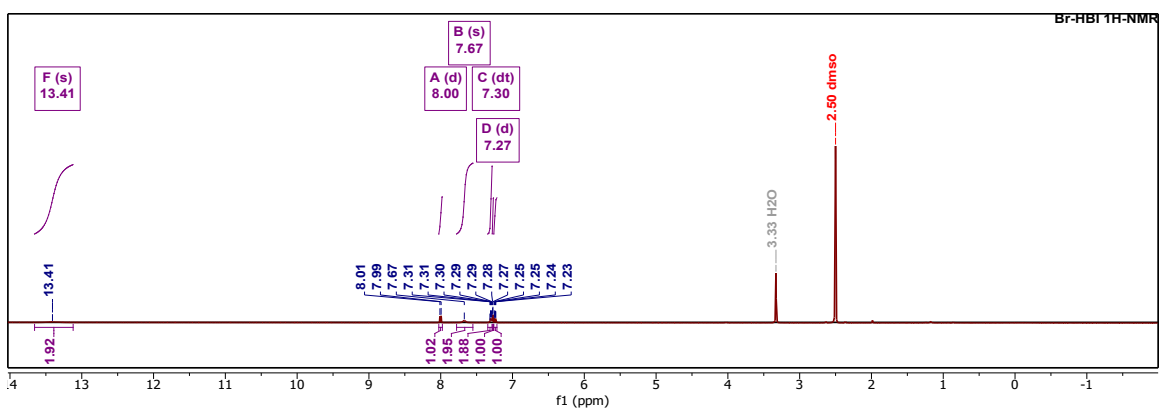
## VII. NMR spectra

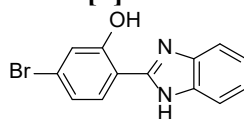
▪ (Br-HBI, 3) 2-(1*H*-benzo[*d*]imidazol-2-yl)-5-bromophenol

Br-HBI

 $^1\text{H}$  NMR (500 MHz, DMSO-*d*<sub>6</sub>)

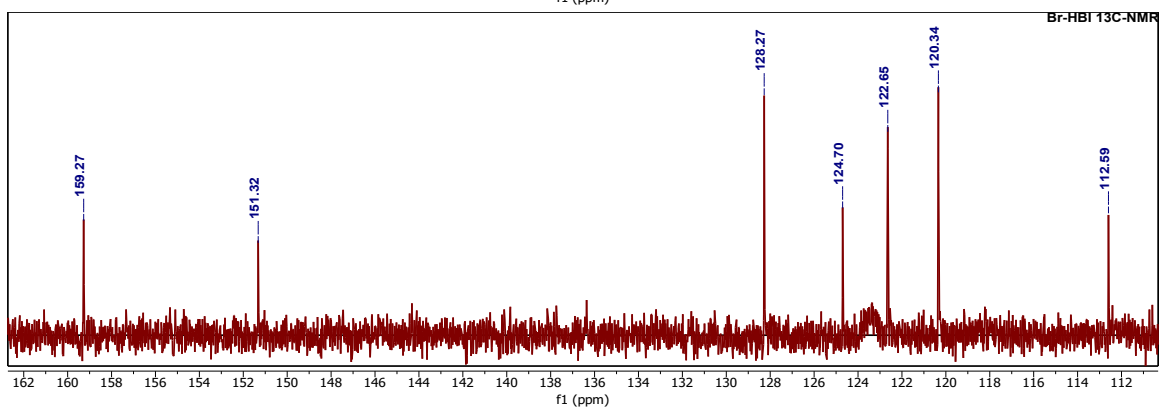
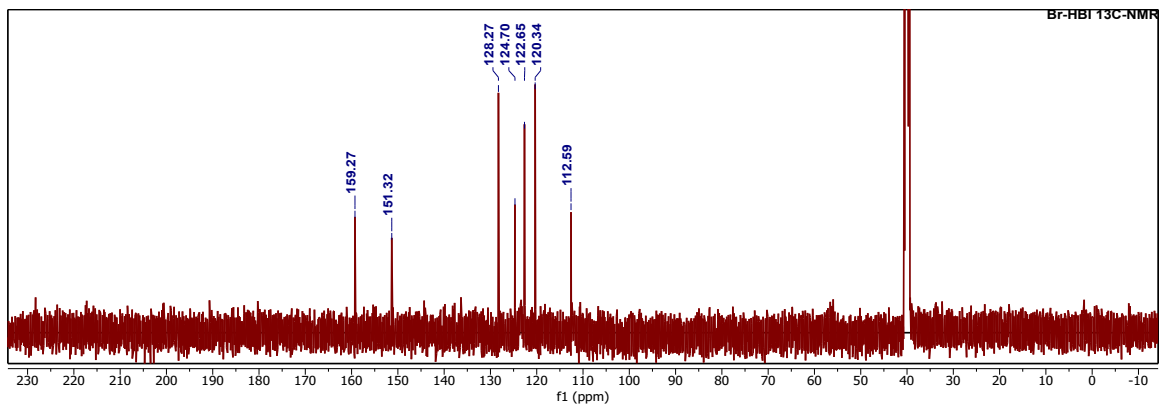
$\delta$  13.41 (s), 8.00 (d,  $J = 8.4$  Hz, 1H), 7.67 (s, 2H), 7.30 (dt,  $J = 6.1, 3.6$  Hz, 2H), 7.27 (d,  $J = 2.0$  Hz, 1H), 7.24 (dd,  $J = 8.4, 2.0$  Hz, 1H).



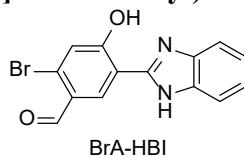
▪ (Br-HBI, 3) 2-(1*H*-benzo[*d*]imidazol-2-yl)-5-bromophenol

Br-HBI

$^{13}\text{C}$  NMR (126 MHz, DMSO-*d*<sub>6</sub>)  
 $\delta$  159.27, 151.32, 128.27, 124.70, 122.65, 120.34, 112.59.

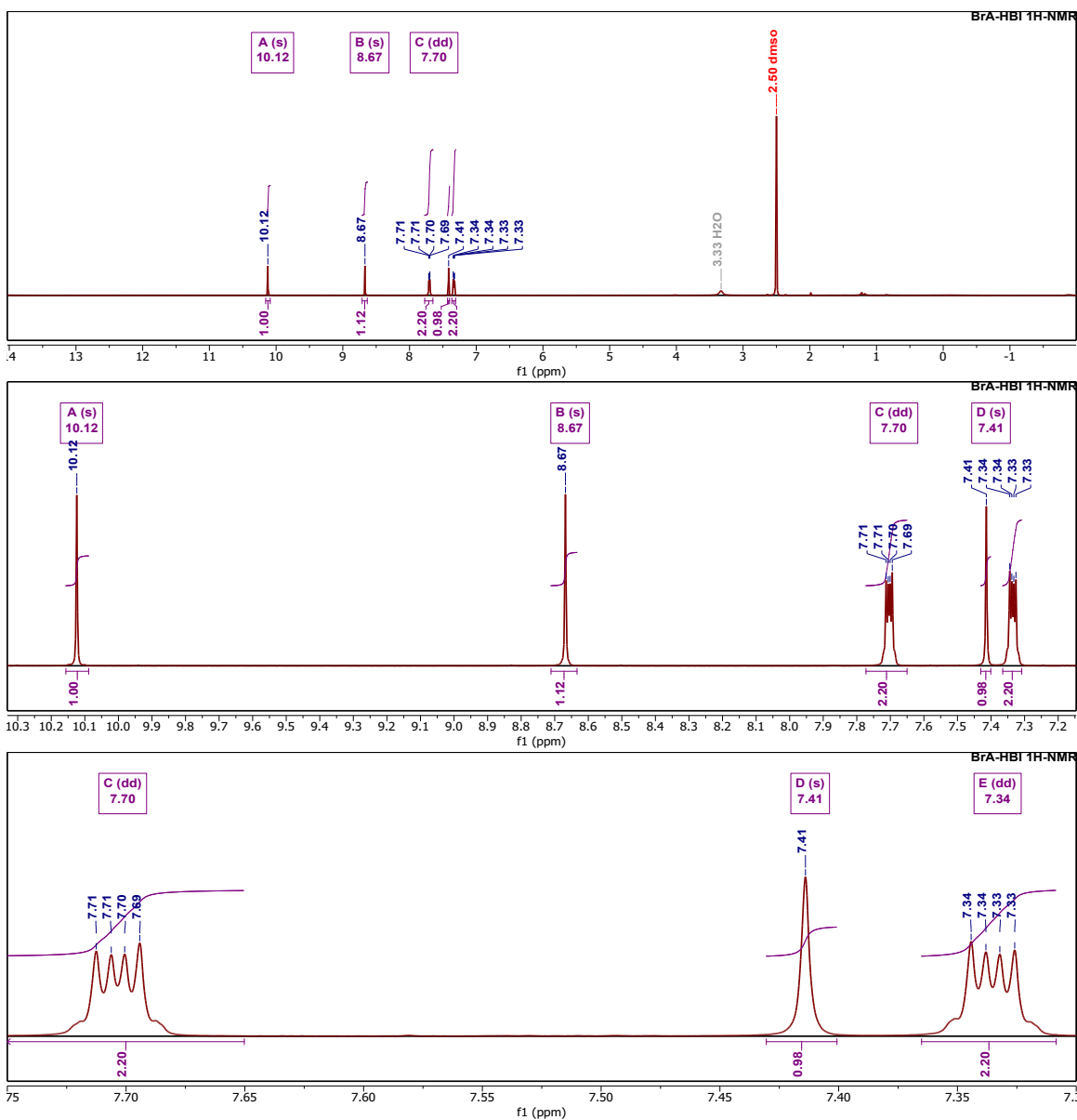


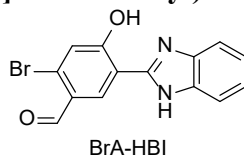
▪ (BrA-HBI, 2) 5-(1*H*-benzo[*d*]imidazol-2-yl)-2-bromo-4-hydroxybenzaldehyde



*<sup>1</sup>H NMR (500 MHz, DMSO-*d*<sub>6</sub>)*

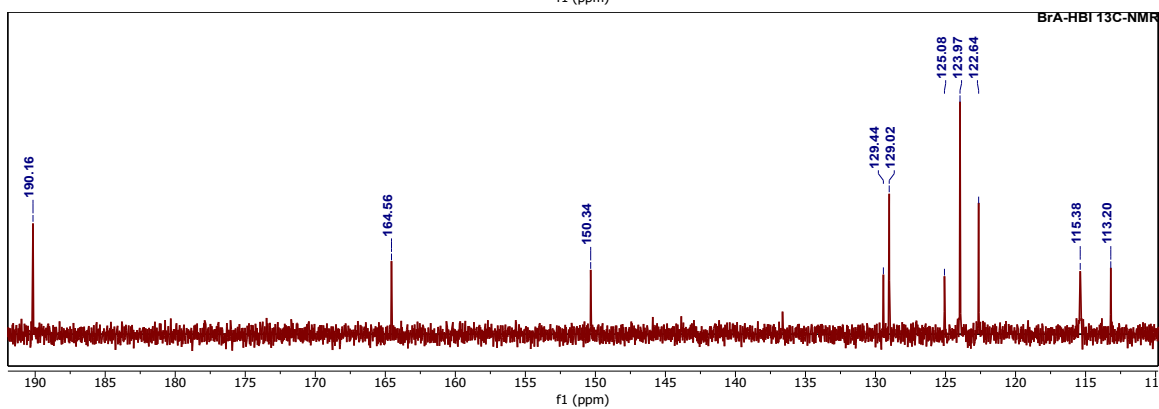
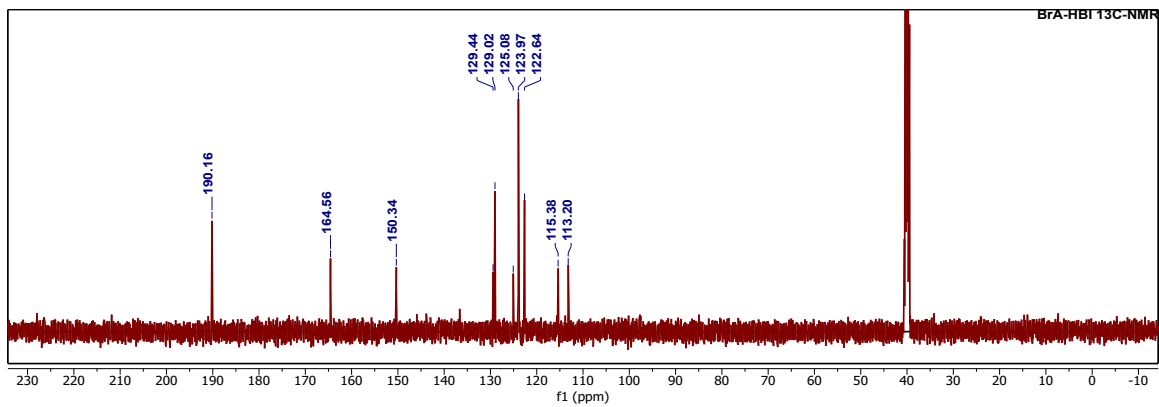
$\delta$  13.41 (s, 2H), 8.00 (d,  $J = 8.4$  Hz, 1H), 7.67 (s, 2H), 7.30 (dt,  $J = 6.1, 3.6$  Hz, 2H), 7.27 (d,  $J = 2.0$  Hz, 1H), 7.24 (dd,  $J = 8.4, 2.0$  Hz, 1H).



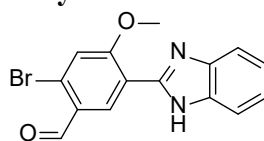
▪ (BrA-HBI, 2) 5-(1*H*-benzo[*d*]imidazol-2-yl)-2-bromo-4-hydroxybenzaldehyde

$^{13}\text{C}$  NMR (126 MHz, DMSO-*d*<sub>6</sub>)

$\delta$  190.16, 164.56, 150.34, 129.44, 129.02, 125.08, 123.97, 122.64, 115.38, 113.20.



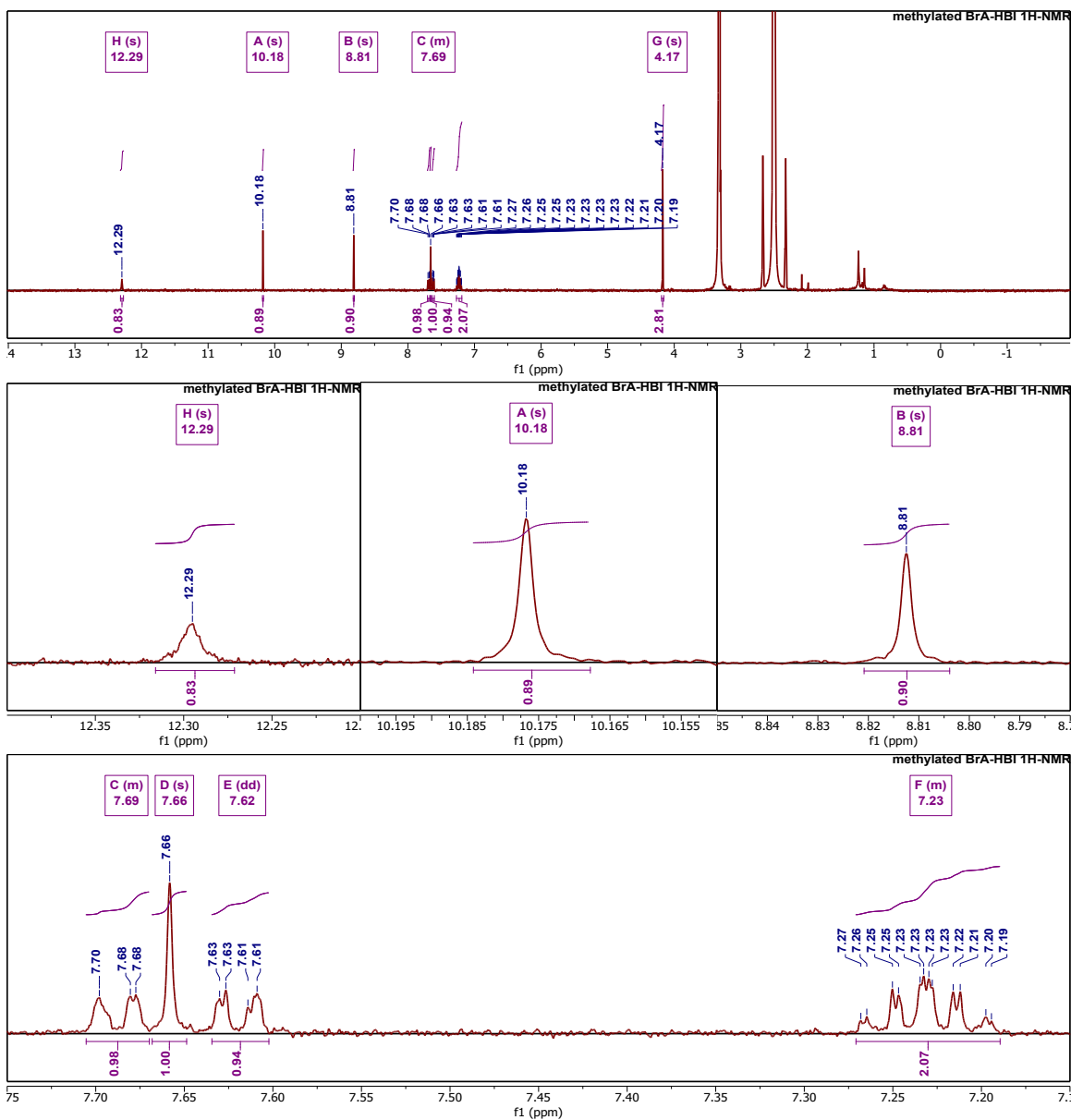
▪ Methylation of BrA-HBI



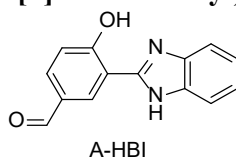
Methylated BrA-HBI

$^1\text{H NMR}$  (400 MHz,  $\text{DMSO-d}_6$ )

$\delta$  12.29 (s, 1H), 10.18 (s, 1H), 8.81 (s, 1H), 7.71 – 7.67 (m, 1H), 7.66 (s, 1H), 7.62 (dd,  $J = 6.7$ , 1.7 Hz, 1H), 7.27 – 7.19 (m, 2H), 4.17 (s, 3H).

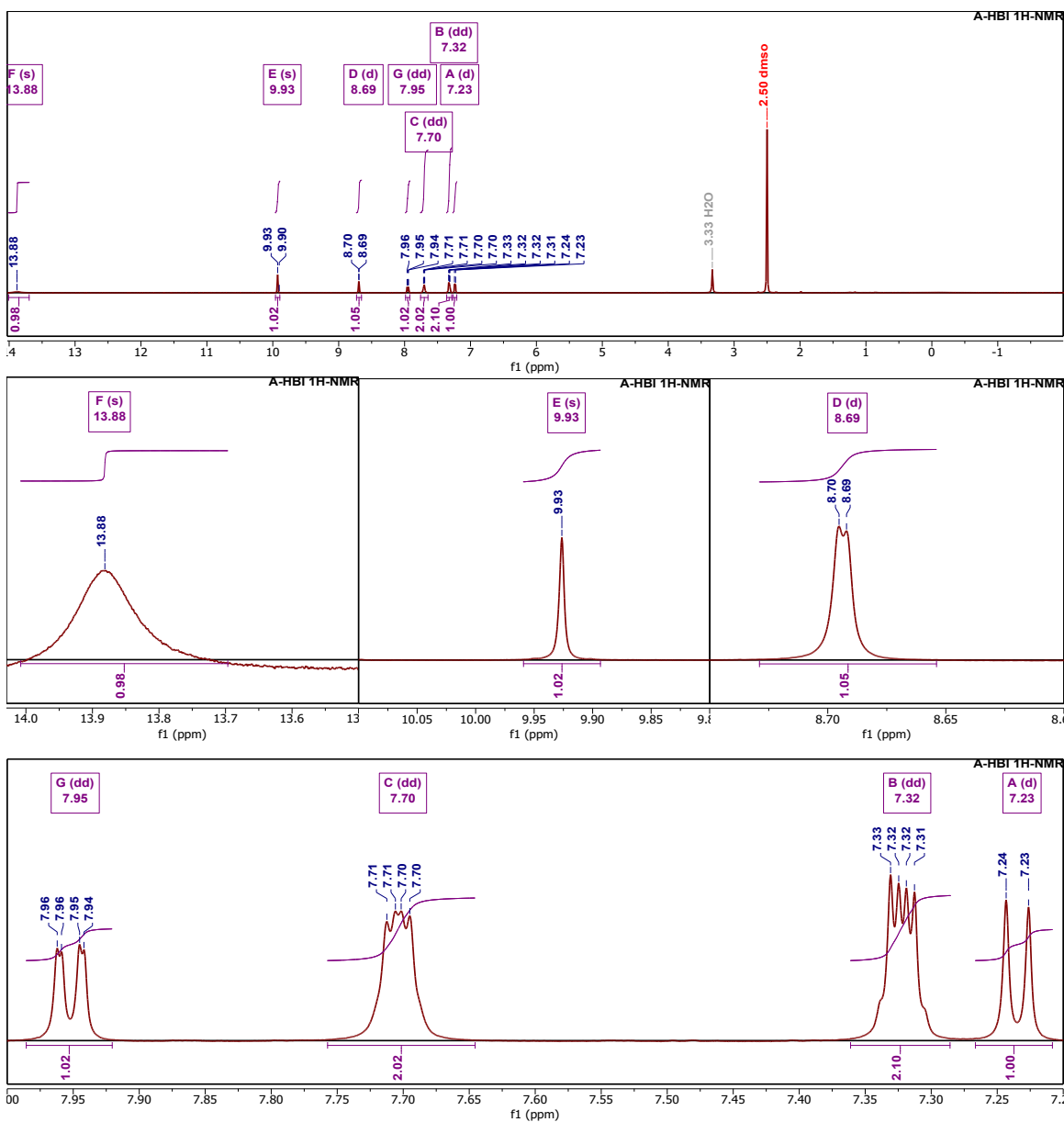


▪ (A-HBI, 4) 3-(1*H*-benzo[*d*]imidazol-2-yl)-4-hydroxybenzaldehyde

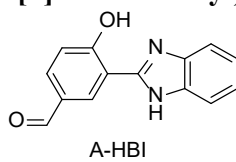


<sup>1</sup>H NMR (500 MHz, DMSO-d<sub>6</sub>)

δ 13.88 (s), 9.93 (s, 1H), 8.69 (d, *J* = 1.6 Hz, 1H), 7.95 (dd, *J* = 8.5, 1.6 Hz, 1H), 7.70 (dd, *J* = 5.4, 3.3 Hz, 2H), 7.32 (dd, *J* = 6.0, 3.1 Hz, 2H), 7.23 (d, *J* = 8.5 Hz, 1H).

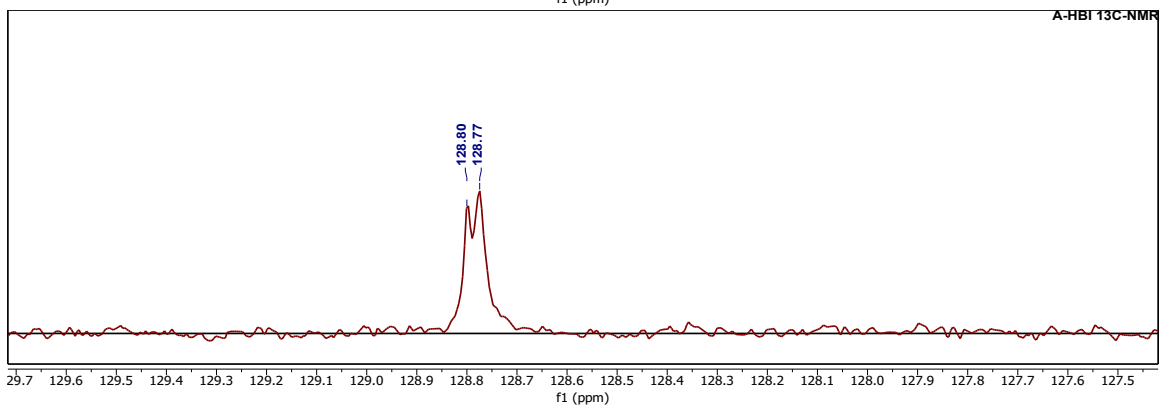
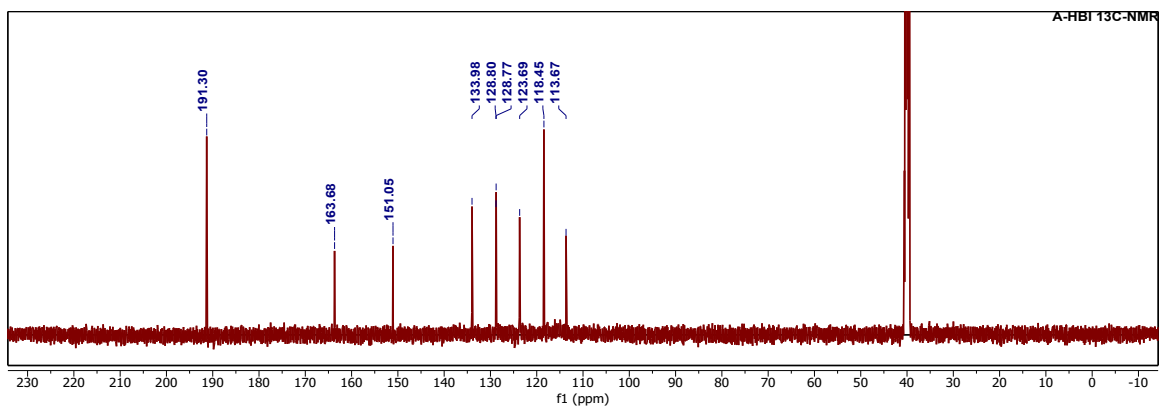


- (A-HBI, 4) 3-(1*H*-benzo[*d*]imidazol-2-yl)-4-hydroxybenzaldehyde

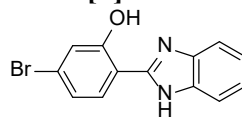


*<sup>13</sup>C NMR (126 MHz, DMSO-*d*<sub>6</sub>)*

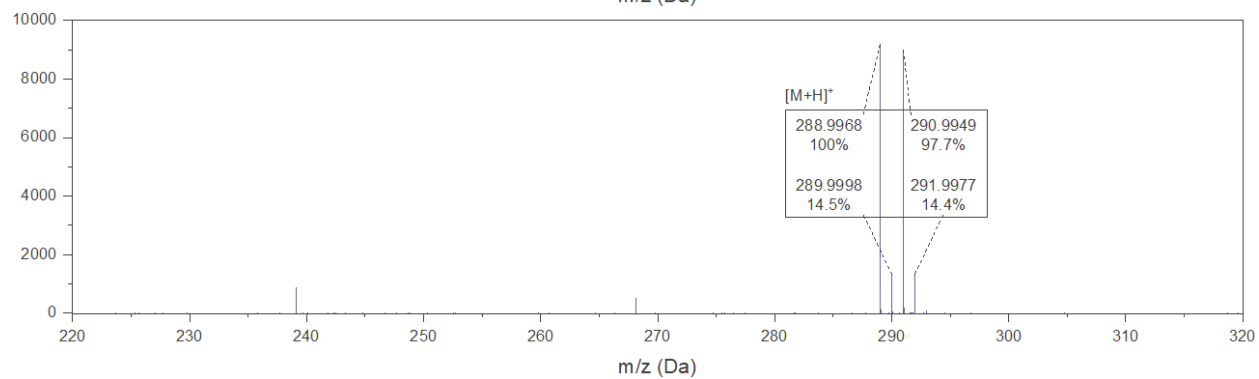
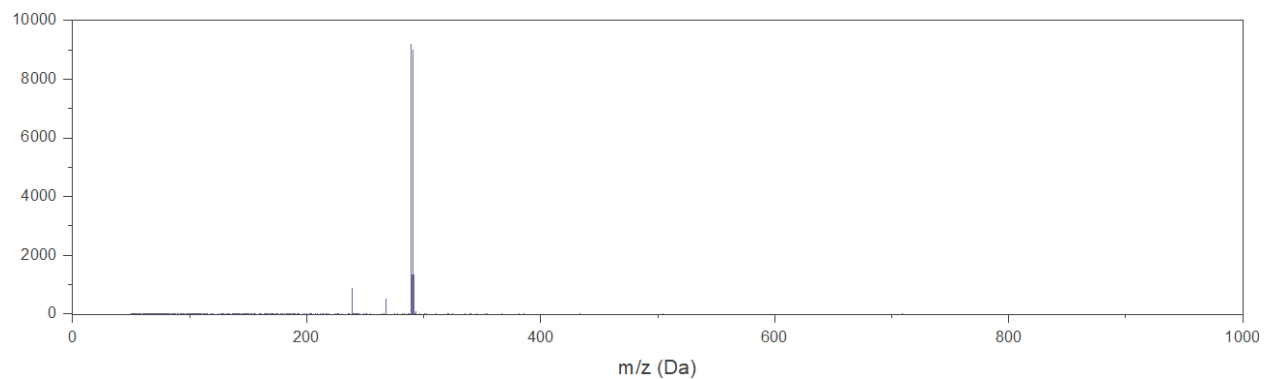
δ 191.30, 163.68, 151.05, 133.98, 128.80, 128.77, 123.69, 118.45, 113.67.



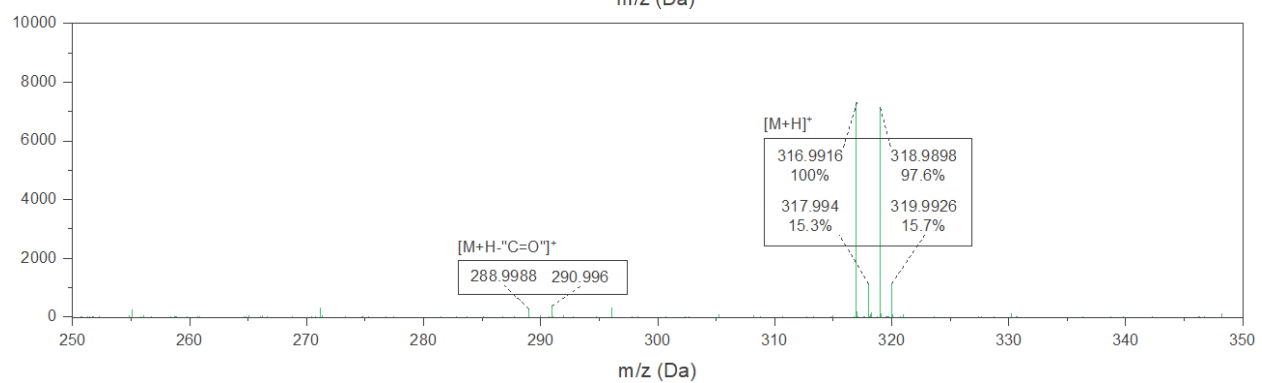
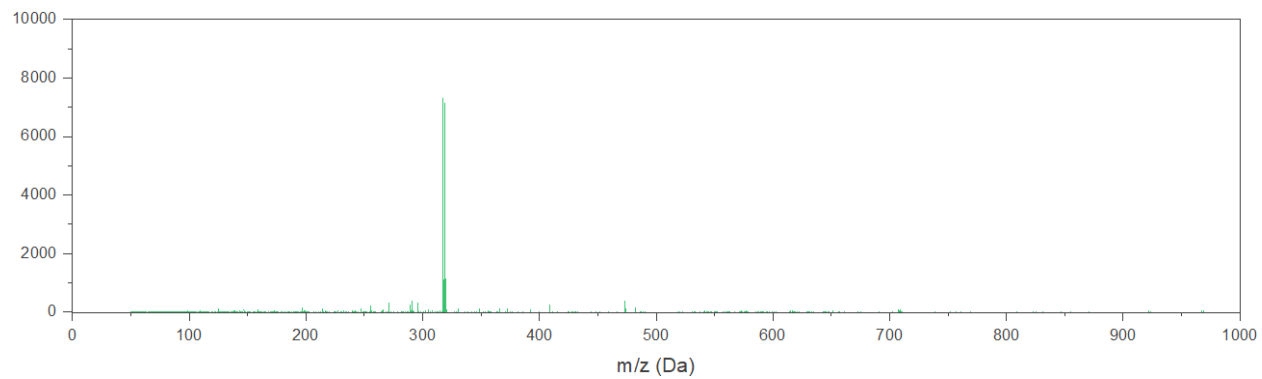
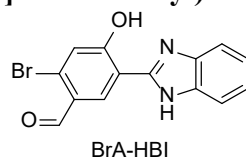
## VIII. Mass Spectra

▪ (Br-HBI, 3) 2-(1*H*-benzo[*d*]imidazol-2-yl)-5-bromophenol

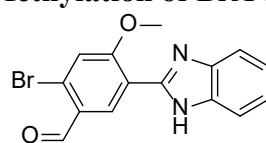
Br-HBI



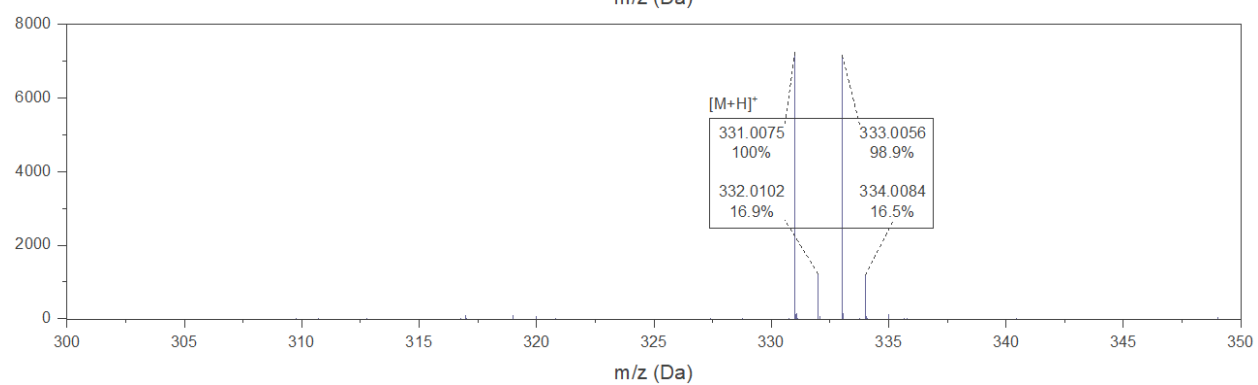
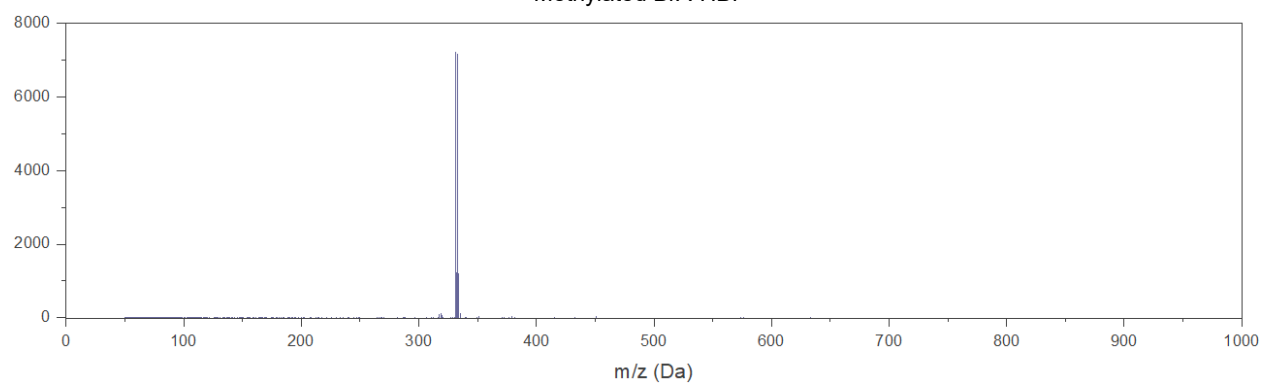


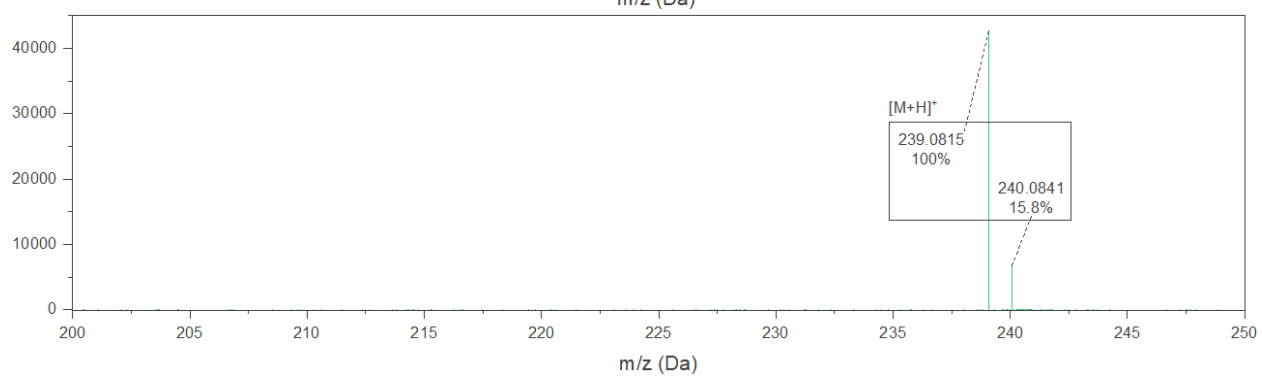
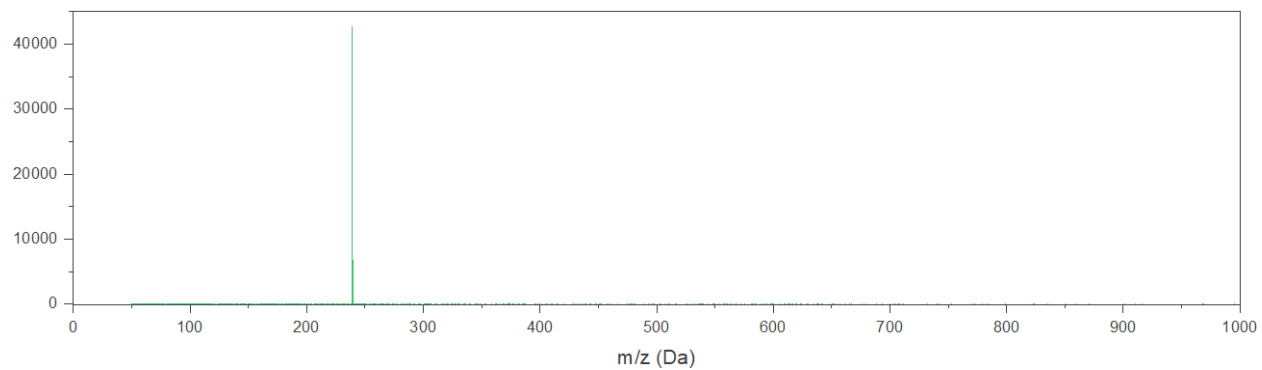
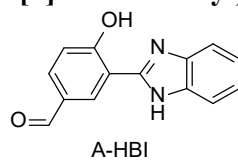
▪ (BrA-HBI, 2) 5-(1*H*-benzo[*d*]imidazol-2-yl)-2-bromo-4-hydroxybenzaldehyde

## ▪ Methylation of BrA-HBI



Methylated BrA-HBI



▪ (A-HBI, 4) 3-(1*H*-benzo[*d*]imidazol-2-yl)-4-hydroxybenzaldehyde

## IX. Reference

- [1] E. Epifanovsky, A. T. B. Gilbert, X. Feng, J. Lee, Y. Mao, N. Mardirossian, P. Pokhilko, A. F. White, M. P. Coons, A. L. Dempwolff, Z. Gan, D. Hait, P. R. Horn, L. D. Jacobson, I. Kaliman, J. Kussmann, A. W. Lange, K. U. Lao, D. S. Levine, J. Liu, S. C. McKenzie, A. F. Morrison, K. D. Nanda, F. Plasser, D. R. Rehn, M. L. Vidal, Z. Q. You, Y. Zhu, B. Alam, B. J. Albrecht, A. Aldossary, E. Alguire, J. H. Andersen, V. Athavale, D. Barton, K. Begam, A. Behn, N. Bellonzi, Y. A. Bernard, E. J. Berquist, H. G. A. Burton, A. Carreras, K. Carter-Fenk, R. Chakraborty, A. D. Chien, K. D. Closser, V. Cofer-Shabica, S. Dasgupta, M. de Wergifosse, J. Deng, M. Diedenhofen, H. Do, S. Ehlert, P. T. Fang, S. Fatehi, Q. Feng, T. Friedhoff, J. Gayvert, Q. Ge, G. Gidofalvi, M. Goldey, J. Gomes, C. E. González-Espinoza, S. Gulania, A. O. Gunina, M. W. D. Hanson-Heine, P. H. P. Harbach, A. Hauser, M. F. Herbst, M. Hernández Vera, M. Hodecker, Z. C. Holden, S. Houck, X. Huang, K. Hui, B. C. Huynh, M. Ivanov, Á. Jász, H. Ji, H. Jiang, B. Kaduk, S. Kähler, K. Khistyayev, J. Kim, G. Kis, P. Klunzinger, Z. Koczor-Benda, J. H. Koh, D. Kosenkov, L. Koulias, T. Kowalczyk, C. M. Krauter, K. Kue, A. Kunitsa, T. Kus, I. Ladjánszki, A. Landau, K. v. Lawler, D. Lefrancois, S. Lehtola, R. R. Li, Y. P. Li, J. Liang, M. Liebenthal, H. H. Lin, Y. S. Lin, F. Liu, K. Y. Liu, M. Loipersberger, A. Luenser, A. Manjanath, P. Manohar, E. Mansoor, S. F. Manzer, S. P. Mao, A. v. Marenich, T. Markovich, S. Mason, S. A. Maurer, P. F. McLaughlin, M. F. S. J. Menger, J. M. Mewes, S. A. Mewes, P. Morgante, J. W. Mullinax, K. J. Oosterbaan, G. Paran, A. C. Paul, S. K. Paul, F. Pavošević, Z. Pei, S. Prager, E. I. Proynov, Á. Rák, E. Ramos-Cordoba, B. Rana, A. E. Rask, A. Rettig, R. M. Richard, F. Rob, E. Rossomme, T. Scheele, M. Scheurer, M. Schneider, N. Sergueev, S. M. Sharada, W. Skomorowski, D. W. Small, C. J. Stein, Y. C. Su, E. J. Sundstrom, Z. Tao, J. Thirman, G. J. Tornai, T. Tsuchimochi, N. M. Tubman, S. P. Veccham, O. Vydrov, J. Wenzel, J. Witte, A. Yamada, K. Yao, S. Yeganeh, S. R. Yost, A. Zech, I. Y. Zhang, X. Zhang, Y. Zhang, D. Zuev, A. Aspuru-Guzik, A. T. Bell, N. A. Besley, K. B. Bravaya, B. R. Brooks, D. Casanova, J. da Chai, S. Coriani, C. J. Cramer, G. Cserey, A. E. Deprince, R. A. Distasio, A. Dreuw, B. D. Dunietz, T. R. Furlani, W. A. Goddard, S. Hammes-Schiffer, T. Head-Gordon, W. J. Hehre, C. P. Hsu, T. C. Jagau, Y. Jung, A. Klamt, J. Kong, D. S. Lambrecht, W. Liang, N. J. Mayhall, C. W. McCurdy, J. B. Neaton, C. Ochsenfeld, J. A. Parkhill, R. Peverati, V. A. Rassolov, Y. Shao, L. v. Slipchenko, T. Stauch, R. P. Steele, J. E. Subotnik, A. J. W. Thom, A. Tkatchenko, D. G. Truhlar, T. van Voorhis, T. A. Wesolowski, K. B. Whaley, H. L. Woodcock, P. M. Zimmerman, S. Faraji, P. M. W. Gill, M. Head-Gordon, J. M. Herbert, A. I. Krylov, *Journal of Chemical Physics* **2021**, *155*, 084801.
- [2] P. C. Hariharan, J. A. Pople, *Theoretica Chimica Acta* **1973**, *28*, 213.
- [3] D. E. Bernholdt, R. J. Harrison, *Journal of Chemical Physics* **1998**, *109*, 1593.
- [4] S. Grimme, *Journal of Computational Chemistry* **2006**, *27*, 1787.
- [5] F. Weigend, R. Ahlrichs, *Physical Chemistry Chemical Physics* **2005**, *7*, 3297.
- [6] P. Pokhilko, E. Epifanovsky, A. I. Krylov, *Journal of Chemical Physics* **2019**, *151*.
- [7] F. Plasser, M. Wormit, A. Dreuw, *Journal of Chemical Physics* **2014**, *141*, 024106.
- [8] G. Schaftenaar, J. H. Noordik, *Journal of Computer-Aided Molecular Design* **2000**, *14*, 123.

- [9] M. Mamada, K. Inada, T. Komino, W. J. Potscavage, H. Nakanotani, C. Adachi, *ACS Central Science* **2017**, *3*, 769.
- [10] K. Wu, T. Zhang, Z. Wang, L. Wang, L. Zhan, S. Gong, C. Zhong, Z. H. Lu, S. Zhang, C. Yang, *Journal of the American Chemical Society* **2018**, *140*, 8877.
- [11] F. Liang, L. Wang, D. Ma, X. Jing, F. Wang, *Applied Physics Letters* **2002**, *81*, 4.
- [12] J. Seo, S. Kim, Y. S. Lee, O. H. Kwon, K. H. Park, S. Y. Choi, Y. K. Chung, D. J. Jang, S. Y. Park, *Journal of Photochemistry and Photobiology A: Chemistry* **2007**, *191*, 51.
- [13] S. S. Y. S. Park, O. H. Kwon, Y. S. Lee, D. J. Jang, S. S. Y. S. Park, *Journal of Physical Chemistry A* **2007**, *111*, 9649.
- [14] A. K. Gupta, W. Li, A. Ruseckas, C. Lian, C. L. Carpenter-Warren, D. B. Cordes, A. M. Z. Slawin, D. Jacquemin, I. D. W. Samuel, E. Zysman-Colman, *ACS Applied Materials and Interfaces* **2021**, *13*, 15459.
- [15] R. M. Khisamov, A. A. Ryadun, T. S. Sukhikh, S. N. Konchenko, *Molecular Systems Design & Engineering* **2021**.